THEORETICAL STUDIES OF STRIPE STATES IN UNDERDOPED CUPRATE SUPERCONDUCTORS

THEORETICAL STUDIES OF STRIPE STATES IN UNDERDOPED CUPRATE SUPERCONDUCTORS

By

SOSHI MIZUTANI, B.SC.

A Thesis

Submitted to the School of Graduate Studies

in Partial Fulfilment of the Requirements

for the Degree

Master of Science

McMaster University

MASTER OF SCIENCE (2016) McMaster University

(Department of Physics and Astronomy) Hamilton, Ontario, Canada

TITLE: Theoretical studies of stripe states in underdoped cuprate superconductors

AUTHOR: Soshi Mizutani, B.Sc.

SUPERVISOR: Dr. Catherine Kallin

NUMBER OF PAGES: xiii, 95

Abstract

In this thesis, we study stripe states in underdoped cuprate superconductors using the Bogoliubov-de Gennes (BdG) method with appropriate models. In non-self-consistent calculations, the nature of stripe states with coexisting unidirectional Pair Density Wave (PDW), Charge Density Wave (CDW), and Spin Density Wave(SDW) order is studied, and it was found that among these coexisting stripe orders, the SDW order plays a key role in reconstructing the Fermi Surface (FS), and the magnitude of SDW order needs to be relatively small in order for Fermi arcs to be realized, while strong SDW order necessarily leads to completely gapped spectra. In self-consistent calculations, we mapped out parameter regions where stripe SC states can be stabilized, which are in qualitative agreement with the generic phase diagram of cuprate superconductors. In addition, self-consistent PDW solutions with small SDW order are stabilized in some parameter region, forming small FS pockets in antinodal regions. This parameter region is a promising one to explore in future work, where self-consistent BdG calculation is to be carried out with a magnetic field in order to study the effect of magnetic field on the stability of stripes along with the possible quantum oscillations.

Acknowledgements

First, I would like to thank my supervisor, Prof. Catherine Kallin, for patiently guiding me through my graduate studies, and also for giving me many opportunities outside of McMaster, such as visiting KITP and attending CIFAR summer school and conference, where I had wonderful experiences. Overall, I was able to improve my research skills, which will be the foundation for my future carrier. I would also like to thank Profs. John Berlinsky, Sung-Sik Lee, and Erik Sorensen for participating in my supervisory committee.

I would also like to thank Wen Huang, for countless discussions on a daily basis. I was very fortunate to share the office with him and learn closely from him. I am hoping that we will stay in touch with each other and talk about physics and all the other things as we have been for the past two years.

I would also like to thank Zeyad Frkash and James Isibor, two of my best friends at McMaster, for always playing soccer and hanging out with me. I hope our tradition of winning will continue, and I also wish all the best for your remaining years at McMaster. I would also like to thank Mr. and Mrs. Muller, for their generous hospitality and treating me as if I am a part of their family.

Lastly, I would like to thank my family. Although they have little idea of what I do, they have been always supportive of my academic pursuits in abroad for the past five years. I cannot thank enough for their unconditional love, which gives me strength to pursue my goals no matter where I am located.

Contents

Chapter 1

Introduction

The main goal of the research presented in this thesis is to study the so called striped superconducting state, a spatially modulated superconducting state that is suggested to exist in cuprates superconductors. Some background on cuprate superconductors is given first in section 1.1. There are many review papers available for more extensive reviews of cuprate superconductors[1, 2, 3, 4]. In section 1.2, an introduction to stripe states in general and the striped superconducting state in particular is given.

1.1 Cuprate Superconductors

Since the discovery of a new superconducting state in Sr-doped La_2CuO_4 with T_c close to 30K in 1986[5], other doped Copper-oxide materials (cuprates) have been found to be superconducting. Cuprate superconductors are classified as high-T_c superconductors (HTS), along with iron-based superconductors discovered in 2006[6].

1.1.1 Lattice Structures

Most high-T_c superconductors with the highest T_c are cuprates with perovskite structure, which consists of the tetragonal or orthorhombic (close to tetragonal) structure composed of 2D copper-oxide layers, separated by a variety of spacing layers along the c (z) direction, which work as charge reservoir layers that provide extra electron or hole carriers on CuO_2 planes upon doping (substituting different ions). The transport between CuO_2 planes along the c direction is very weak, hence they are classified as quasi-2D systems; series of 2D layers stacked in the c direction, which are only weakly coupled. These are the generic features of all the cuprate families, which reduces the problem of understanding high temperature superconductivity in the cuprates largely to understanding the physics of strongly correlated CuO_2 layers as we see in the next section. Different cuprate families tend to be used in different experiments due to their particular properties, but the data and conclusions based on different families are usually put together to make some general statement about the entire cuprate family.

1.1.2 CuO_2 planes

It is widely, although not universally*, accepted that the essential physics of the cuprates can be captured in a single band, tight binding model with appropriate local interactions[8, 9, 10]. Only the $3d_{x^2-y^2}$ orbital is considered in the model, while all the other lower energy 3d orbitals of Cu and 2p orbitals of O are filled and neglected. Within the tight-binding description with a single band provided by $3d_{x^2-y^2}$ orbitals on the Cu sites, all the physics is simplified to particles hopping between sites on a square lattice with magnitude given as a

* There are some studies which consider the three-band Hubbard model which includes p orbitals at O atom site, where some interesting properties that can't be explained in a single band model such as orbital currents are found[7].

function of the distance and direction of the hopping. Without doping, the band is half-filled, i.e. each site is occupied with one electron, but particle/hole doping on CuO_2 planes changes the local carrier density, hence leaving some sites empty or doubly occupied. Note that, generally, in the band theory picture, one would expect the system to be metallic with a half-filled conduction band, but in reality, the undoped cuprates are an antiferromagnetic insulator with a Neel temperature of $T_N \simeq 280K$, which results from strong electron correlations[4]. This is called a Mott-Hubbard insulator[11], and in order to account for the strong correlations in this Mott-Hubbard insulator, appropriate local interactions must be included in the single-band, tight-binding model, as in the Hubbard and t-J model, which are two of the most studied models for cuprates that can realize various orders such as antiferromagnetic (AF) order and superconducting (SC) order. The details of the specific models used in this thesis are discussed in Chapter 2.

1.1.3 Phase diagram

The Fermi Liquid ground state that describes conventional metals turns out to be quite unstable in strongly correlated electron systems, especially in low dimensional ones. Such systems give rise to various (Fermi surface) instabilities, and the system energy can be lowered by opening a gap at Fermi level through the formation of various orders such as antiferromagnetism (AF), superconductivity (SC), Charge Density Wave (CDW), and Spin Density Wave (SDW), which are all stabilized by some type of interactions.

Cuprate superconductors have been one of the most studied correlated electron materials, both theoretically and experimentally, and the phase diagrams for these materials as a function of temperature and electron or hole doping are very rich and complex, with many different phases existing with similar T_c. This phenomenology of multiple orders with similar transition temperatures and which coexist in parts of the phase diagram has inspired the term "intertwined order" by Kivelson, Fradkin and others[1]. Turning to the theoretical models, this near degeneracy of multiple orders, on the one hand, makes the identification of the true ground state extremely difficult, on the other hand, it implies that the t-J model in the physically relevant regime is at or close to a phase transition between competing phases. Consequently, small additional and/or anisotropic terms in the model can stabilize one phase over the others. Since these additional terms will depend on the details of cuprate compounds, this can explain, for example, why stripes are only found in certain cuprates. Experimentally, the exact details of the cuprate phase diagrams may differ depending on the type of experimental techniques and samples used. However, there is a consensus on some generic behaviors of the phase diagram, which are depicted in Fig. 1.1, a typical phase diagram for cuprate superconductors, where the definition of each phase is given in the caption.

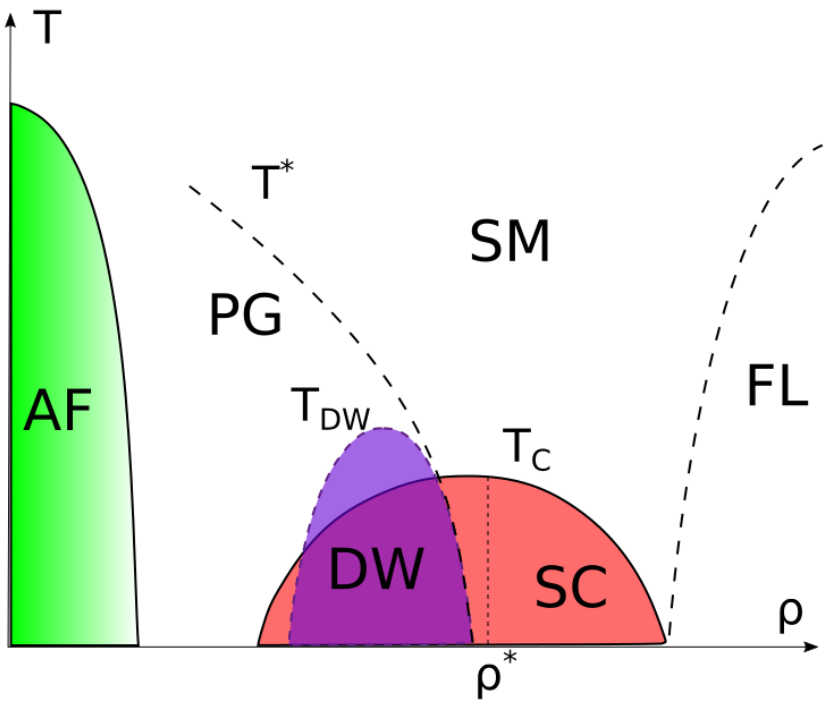

Figure 1.1: A typical temperature (T) vs hole-doping (ρ) phase diagram for the non-La-based cuprates.The ground state of the undoped parent compound is an antiferromagnetic (AF) Mott insulator, which upon hole doping leads to a d-wave superconductor (*SC*) with transition temperature T_c. The highest T_c is achieved at the optimal doping ρ^*, the doping range below (above) which is called the underdoped (overdoped) region respectively. The familiar Fermi-Liquid (FL) behavior appears at the extreme overdoping region. The two mysterious phases are the pseudogap (PG), which onsets at a high temperature (T*), and the strange-metal (SM). Inside of the PG phase at the lower temperature ($T_{DW} < T^*$) exists a density-wave (DW) phase, where some type of short-range charge density wave order is observed. The CDW is probably stripe like, although there is some ongoing discussion of whether it is 2d or 1d like.

1.1.3.1 Pseudogap phase

Among the various phases in the phase diagram given in Fig. 1.1, the pseudogap phase, which shows Non-Fermi-liquid-like behavior, is a particularly mysterious phase. "Non-Fermi-liquid-like" here means that, unlike the Fermi liquid behavior observed in most metals, the sharp fermionic excitations are broadened even close to the Fermi Surface[12, 13] The gapless spin excitations are suppressed as seen by NMR experiments[14], leading to a suppressed

but nonzero density of states (DOS) at the Fermi level[15], i.e. this gap is not a full gap, but a partial gap, therefore the name, pseudogap. The source of the pseudogap is not well understood, and different theories view it as, among other possibilities, a form of order, or a density wave competitor to SC, or a remnant of SC with phase-incoherent Cooper pairs without long range order[16]. The complete understanding of the nature of psuedogap is yet to be accomplished, which is considered to be a key to constructing a theory for the mechanism of high T_c superconductivity in the cuprates. More specifically, understanding the electronic properties of the non-Fermi-liquid normal states around the pseudogap region and how they give rise to the SC phase is one of the key issues to be resolved.

1.1.3.2 Fermi Arcs observed by ARPES

The appearance of "Fermi arcs" observed by angle-resolved photoemission spectroscopy (ARPES) is one of the key experimental signatures for the psuedogap phase[17]. Fermi arcs are line segments in momentum space centered near the four (d-wave) nodal points at diagonals where zero-energy excitations can occur, while anti-nodal regions are gapped out or at least do not have any well-defined low energy electronic quasiparticles.(Fig. 1.2). The length of the arcs is reduced with decreasing T, consistent with shrinking to the nodal points in the $T \to 0$ limit, where the uniform d-wave superconductivity (dSC) is expected[18].

1.1.3.3 Quantum Oscillations

Quantum oscillations (QO) is another important experimental technique, which is used to map the Fermi surface of a metal in the presence of a magnetic field at low temperatures. Various experimental measurements on metals in strong magnetic fields, such as resistance

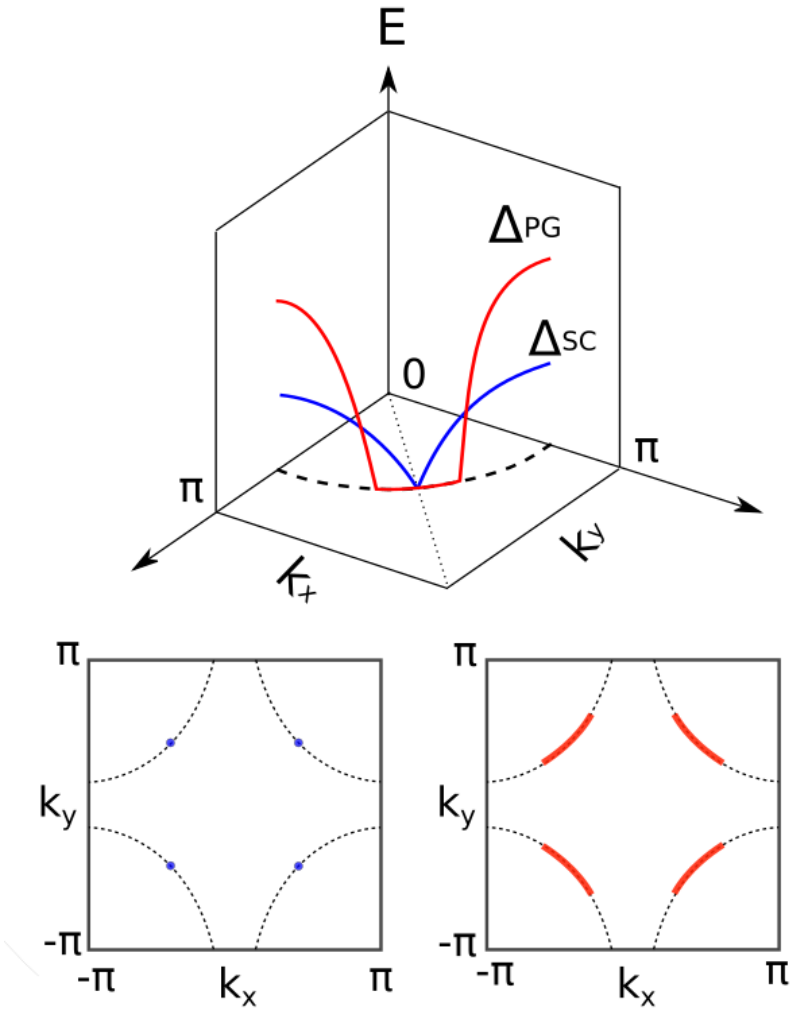

Figure 1.2: (Top) The angle dependence of the superconducting gap Δ_{SC} (blue line) and the effective pseudogap Δ_{PG} (red line) overlayed on the large Fermi surface (dashed curve) shown in one quadrant of the First Brillioun zone (FBZ). (Bottom Right) The Fermi arcs observed in the pseudogap phase. (Bottom Left) The four nodal points of the uniform dSC state. These arcs may get reconstructed into small pockets at the nodal regions once charge order with the wave vector $\mathbf{Q} = (Q,0)$ sets in, as revealed by QO measurements. Note that the origin of the effective peudogap Δ_{PG} which produces the Fermi arcs is not well understood.

(the Shubnikov-de Haas effect), Hall resistance, and magnetic susceptibility (the de Haas-van Alphen effect), exhibit oscillatory behavior as a function of the inverse of magnetic field strength, and based on the frequency of such oscillations, the area of underlying Fermi Surface can be calculated (The detailed theory of QO are given in condensed matter text books such as [19, 20]). A superconductor typically exhibits QO at low temperatures for magnetic fields that are sufficiently close to or above the upper critical field, H_{c2}. For the cuprates, quantum oscillations in the underdoped cuprates were first observed in the electrical resistivity of YBCO in 2007[21], and since then, QO have been observed in various other measurements and are now a well-established phenomenon in the cuprates[22, 23, 24, 25, 22, 26, 27], which suggests the existence of small closed Fermi pockets in the normal state of the underdoped cuprates[†]. More careful recent experiments[28] see the oscillations expected for a small closed pocket to coincide with doping regimes where some type of charge order is seen. Note that the Fermi arcs observed by ARPES and the small closed Fermi pockets suggested by QO seem to contradict each other, but one possible scenario is that ARPES observes only one side of the pocket with significant weight, and the arcs could be just a piece of a Fermi pocket[‡]. The problem in this scenario, however, is that the existing pocket then would be too large to quantitatively explain the observed QO. Other possible scenarios are, among others, that QO experiments only see one pocket despite the existence of multiple pockets, or that QO might in fact be

[†] Here, what is meant by 'normal' state is ambiguous, since QO measurements are performed in a resistive state where the superconducting paring, however, can still be present if the magnetic field is below H_{c2} and the sample is in a vortex liquid state which gives rise to finite resistivity. Note also that the application of strong magnetic field necessary for QO measurements itself might alter the respective stability of various states observed in underdoped region, which is one of the important research directions.

[‡] Small electron pockets at the anti-nodal region is also likely in this scenario, but ARPES may not see this only because they are incoherent, or in more technical many body language, the quasiparticle renormalization factor z is small, where $z = 1$ means free electron like and $z = 0$ means no electronic quasiparticles, and sections with small z are generally hard to see with ARPES, which detects a real electron extracted by the photo emission.

consistent with multiple pockets through some theoretical explanation. Overall, it remains an unexplained puzzle exactly what the Fermi surface is in the underdoped regime.

1.2 Stripe states

The definitions of some terms regarding stripe states, which are particularly important in this thesis but often used ambiguously in different contexts, are clarified here;

- Density wave (DW): a periodic modulation of some local parameters, such as charge density $n_i = n_{i\uparrow} + n_{i\downarrow}$, magnetization $m_i = n_{i\uparrow} - n_{i\downarrow}$, and pair density Δ_i, corresponding to Charge Density Wave (CDW), Spin Density Wave (SDW), and Pair Density Wave (PDW) respectively. Note that the periodicity and direction of DW is defined by the wave vector $\mathbf{q}$, which is unidirectional for stripe-like DW.

- Stripe state: a state with unidirectional density wave(s), such as CDW, SDW, PDW, or combination of these. The physical properties of a stripe state, such as whether it is metallic or superconducting, depend on the type of DW(s) present and their relative magnitudes and configurations, but by "stripe state", it typically means non-superconducting stripe unless otherwise mentioned. The terms "charge stripe" and "spin (or magnetic) stripe" are also used to refer to the unidirectional CDW and SDW respectively.

- Pair Density Wave (PDW): In this thesis, PDW or stripe SC is used, by default, for the stripe-like PDW order which has no uniform SC component and therefore with a sign change in Δ_i across the anti-phase domain walls, and the concomitant CDW and SDW are presumed unless otherwise stated.

- modulated d-wave SC (mdSC): a special case of PDW with finite uniform SC component, which is usually larger than the magnitude of the modulation, hence Δ_i oscillates around the uniform component without a sign change.

1.2.1 Introduction

As seen in the previous section, the undoped parent compounds of the high T_c cuprates are neither metallic nor superconducting in the ground state, but instead they are AF Mott insulators[11], where both the AF and the insulating behavior are due to strong electron-electron interactions. In order to induce SC, hole doping is necessary, which disrupts the originally half-filled, long range AF order. Unlike in conventional metals and insulators, where the energy scale in the system is set by the kinetic energy and potential energy of interactions respectively, in the doped cuparates, both kinetic and potential energy need to be considered on equal footing, since even though the short range repulsive interaction is still the largest in energy, the ground state shows a rich structure in both real and momentum space, hence neither of them is a good quantum number. For example, while concentrating all the injected holes at one region would minimize the area where the original AF order is disrupted, therefore minimizing the energy cost associated with loss of AF condensation energy, this configuration would come with a high energy cost due to the long range Coulomb repulsion between the concentrated holes, and it would also come with higher kinetic energy. As a compromise between the AF interactions, the long range Coulomb interactions, and the kinetic energy, numerical studies of simple models thought to describe the cuprates find that the optimum configuration in the lightly hole-doped Mott insulator is a stripe structure, where the doped holes are concentrated along spontaneously generated domain walls between AF insulating region. In other words, stripe states come with unidirectional CDW and SDW order. Such stripe behavior is also seen in some parts of the phase diagram in some cuprate materials. This stripe configuration is schematically depicted in Fig. 1.3, and the charge and spin stripes are mostly observed near $x = 1/8$ hole doping, although they are also observed over a broader doping in some cuprate materials (more details in section 1.2.2).

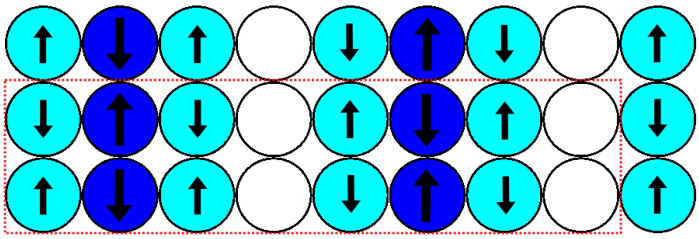

Figure 1.3: A schematic picture of a stripe state with coexisting charge and magnetic stripe (unidirectional CDW and SDW order) in the 2D square lattice, where three-legged AF spin ladders are separated by non-magnetic metallic lines. Each circle represents a (Cu) site in the lattice, and the arrows represent the amplitude and direction of the spin density $m_i = n_{i\uparrow} - n_{i\downarrow}$, and the shading of the circles represents the charge density $n_i = n_{i\uparrow} + n_{i\downarrow}$ (the darker circle corresponds to the higher charge density). Note that non-magnetic metallic lines (the vertical lines of white circles) form the anti phase domain-wall, across which the AF stripes change the sign. A unit supercell of size $(l_x, l_y) = (8, 2)$ is also indicated by the red dashed lines.

The importance of the stripe phase with regard to SC in cuprates is suggested naturally due to the proximity of the two phases. The major difficulty in understanding cuprate superconductors come from the fact that there is no consensus on the nature of the underdoped normal state from which the superconductor condenses. The stripe state is one of the candidate states which might play a key role for understanding some properties of the underdoped cuprates.

1.2.2 Experimental studies of stripes

Experimentally, the most direct evidence for (charge) stripes comes from neutron scattering studies [§], where extra Bragg peaks appear due to the new periodicity of stripes and the position and magnitude of the new peaks provide a measure of direction, periodicity, and amplitude of the modulation in stripes. For spin stripes, the long-period incommensurate SDW was first observed by inelastic neutron scattering of superconducting $La_{2-x}Sr_xCuO_4$ (LSCO). Later, Tranquada et.al. suggested, based on their neutron scattering data, a particular form

[§] Note that neutrons which have neutral charges are scattered by the underlying ionic displacements (also studied with electron and x-ray diffraction) induced by the charge modulation

of coexistent charge and spin stripes in hole-doped cuprates, with three-legged AF spin ladders separated by metallic lines, as shown in Fig. 1.3. The doping region over which spin and/or charge order is seen, as well as the correlation length of the order, typically increases if a magnetic field is applied[29]. The hole-rich, non-magnetic metallic lines form anti-phase domain-wall boundaries between the almost half-filled AF stripes. Near $x = \frac{1}{8}$ hole-doping, SDW order is enhanced while SC is suppressed, and unusual behavior in various measurements are also observed, hence called "$\frac{1}{8}$ anomaly"[30].

Quantum oscillations in the underdoped region of some cuprate materials is also taken as indirect evidence of charge order, since the quantum oscillations are consistent with small Fermi pockets of a reconstructed FS. The details of connecting QO experiments to specific order, whether stripes or two-dimensional order, is an active field of investigation and it is still an open question as to exactly what order is needed to explain these experiments[31, 32, 29].

1.2.3 Theoretical studies of stripes

Historically, the existence of charge and spin stripes was theoretically predicted for cuprates even before their experimental discovery. The AF stripe formation was first found in MF solution of a two-band Hubbard model[33, 34], and after the experimental discovery of stripes, the concept of a striped phase, one-dimensional hole rich chains separating stripes of AF order, was developed by a number of theoretical groups, using the Hubbard, t-J and related models[35, 36, 37, 38]. The single-band t-J model was found to be a useful approach for the stripe formation in hole-dope cuprates, and it was then studied extensively by various numerical methods such as exact diagonalization[39], density matrix renormalization group (DMRG) methods[40, 41, 42], Monte Carlo simulations[43], all of which point to the stripe formation in t-J model.

A stripe SC state, where Cooper pairs with finite center-of-mass momenta $\mathbf{q}$ and $-\mathbf{q}$ coexist, hence forming the Pair Density Wave (PDW) with the wave vector $\mathbf{q}$ was suggested to explain some of the observed properties of striped cuprates, especially the $1/8$ annomaly, and consequently the stipe SC state is studied mostly around this doping range. Note that while the existence of a non-SC phase with static charge or magnetic stripes is reasonably well-established as seen in section 1.2.2, the direct evidence of stripe SC state is not found yet. The best experimental motivation to study these states are the decoupling effects in a magnetic field seen near $x = 1/8$, which can be explained with the PDW state[44].

Stripe SC states (PDW and mdSC) have been found in several mean-field theories of the t-J and related models[43, 45, 46, 47, 48]. In a series of studies especially related to this thesis[49, 50, 51], where a $t - t'$ tight binding model with a realistic FS for cuprates with attractive nearest neighbor interaction V is studied in the framework of a BCS mean-field theory using a self-consistent BdG calculation, it is found that the PDW and mdSC state can be stabilized as a self-consistent solution, but only for fairly large attractive interaction $V = 1 \sim 3$, while the uniform d-wave SC state is found for small V, which is consistent with the findings in earlier studies of the t-J model using variational Monte Carlo simulations[43, 45] and mean-field theory[46]. The fact that the fairly large attractive interaction V is necessary to stabilize stripe SC states is, on one hand, somewhat understandable, since no generic band structure has a divergent PDW susceptibility, but on the other hand, the physical plausibility of such large effective attractive interaction in actual systems is somewhat questionable.

One possible mechanism of the formation of stripe SC is based on the effect of a magnetic field that may stabilize stripe SC, since the pinning effect of magnetic field is to enhance both CDW and SDW order, which are intertwined with PDW order. In addition, upon introducing magnetic field and hence driving the system into the mixed state, a stripe SC state can accom-

modate vortices with lower cost in vortex core energy than a uniform SC state, since there are already zeros in the SC order parameter where the resulting vortices can sit. In these contexts, the PDW state in the presence of magnetic field was studied using a non-self-consistent BdG calcuation[48, 52], where it is found that the pockets of Bogoliubov quasiparticles of the PDW state can give rise to quantum oscillations (QO) in the mixed state in an approximation which neglects the effects of vortices, and the area of the pockets are consistent with some experiments. In general, the observation of QO is associated with closed pockets, hence it was originally unexpected for the pseudogap region, where the Fermi arcs, 1D sections of FS, are observed. One possible explanation is that stripe SC states, due to their translational symmetry breaking, reconstruct the FS into small electron and hole pockets located at anti-nodal and nodal regions respectively, and in the PDW state, the hole pockets give rise to the QO, while the electron pockets are gapped out by the PDW order, and the observation of the Fermi arcs can be understood as experimental measurements such as ARPES are only detecting one side of the hole pockets with significant spectral weights. On the other hand, the pockets formed by a PDW are mixtures of quasiparticles and quasiholes, and so it is not clear that they give rise to QO beyond the approximation used by Zelli. In any case, the nature of the Fermi surface and arcs versus pockets is investigated in Chapter 4 and 5 of this thesis.

The rest of this thesis is organized as follows. In chapter 2, theoretical models used in this thesis to study the stripe SC states in cuprates are introduced. In chapter 3, the construction of the self-consistent BdG calculation, a numerical method used in this thesis, is introduced. In chapter 4, the results of the non-self-consistent BdG calculation for the stripe SC states are presented to qualitatively understand various stripe states. Upon gaining some insights from chapter 4, the results of the self-consistent BDG calculation of stripe SC states, the main results of this thesis, are presented in chapter 5. These results both reproduce and extend the works of Loder and others[47, 49, 50] by determining the phase diagram in doping and

parameter space where the PDW state is stable in BdG. Finally, in Chapter 6, some concluding remarks on the results and open questions are made.

Chapter 2

Models

In this chapter, the two different microscopic models, the extended t-J model ($t-J$ model with on-site repulsive Coulomb interaction) and the extended Hubbard model (UV-model), are introduced in section 2.1 and 2.2 respectively, and the qualitative similarity of the two models is shown at mean-field level. Upon establishing the bridge between two models, the UV-model will be used for the numerical calculations and subsequent discussion.

2.1 Hubbard model and tJ-model

The Hubbard model and t-J model are the most studied models for cuprate superconductors, and they are believed to contain many of, if not all of, the important physics observed in the cuprate[53].

The Hubbard model is defined as[54] *,

* For the rest of this thesis, $\sum_{\delta}$ (the sum over all the nearest neighbors) notation will be used rather than $\sum_{\langle i,j\rangle}$ (the sum over all the bonds) notation;

$$\sum_{\langle i,j\rangle} A_i A_j = \frac{1}{2}\sum_{i,\delta} A_i A_{i+\delta}$$

, where A_i is any local operator at site i, and δ corresponds to the four nearest neighbors on 2D square lattice, $\delta = \pm\hat{x}, \pm\hat{y}$. δ in the hopping term shall be used to include the next-nearest neighbors as well if mentioned so.

$$\mathcal{H}_U = -\sum_{i,\delta,\sigma} t_\delta c^\dagger_{i,\sigma} c_{i+\delta,\sigma} + U \sum_i n_{i\uparrow} n_{i\downarrow}, \tag{2.1}$$

the strong U limit of which leads to the t-J model,

$$H_{t-J} = -\sum_{i,\delta,\sigma} t_\delta \hat{c}^\dagger_{i,\sigma} \hat{c}_{i+\delta,\sigma} - \mu \sum_{i,\sigma} n_{i,\sigma} + \frac{J}{2} \sum_{i,\delta} \left(\mathbf{S_i} \cdot \mathbf{S_{i+\delta}} - \frac{n_i n_{i+\delta}}{4} \right), \tag{2.2}$$

where $\hat{c}_{i,s} = c_{i,s}(1 - n_{i,-s})$ is the projected annihilation operator which disallows the double occupancy on site i, and δ is typically constrained to nearest-neighbors (nn) or to nn and next-nn (nnn) only. The spin operator is $\mathbf{S_i} = \sum_{s,s'} c^\dagger_{is} \hat{\sigma}_{ss'} c_{is'}/2$ with the Pauli matrices $\hat{\sigma} = (\sigma^x, \sigma^y, \sigma^z)$. The complexity due to the double occupancy constraint enforced by the projected operators is the major obstacle in solving the t-J model.

Kagan and Rice introduced a way to go around this obstacle to solve the t-J model, by using the extended t-J model[55],

$$H_{t-J-U} = -\sum_{i,\delta,\sigma} t_\delta c^\dagger_{i,\sigma} c_{i+\delta,\sigma} - \mu \sum_{i,\sigma} n_{i,\sigma} + \frac{J}{2} \sum_{i,\delta} \left(\mathbf{S_i} \cdot \mathbf{S_{i+\delta}} - \frac{n_i n_{i+\delta}}{4} \right) + U \sum_i n_{i\uparrow} n_{i\downarrow}, \tag{2.3}$$

where the conventional c operators replaced the projected c operators, and an additional Hubbard repulsion term is introduced to enforce the local constraints. In $U \to \infty$ limit, (2.2) and (2.3) become equivalent, since the infinitely large U disallows double occupation at each site. However, in the strong U limit, the magnitude of the overestimation of AF order over SC order in the mean-field solutions becomes stronger in (2.3) than (2.2) (Kampf et al., 2008). Hence,

choosing the proper U in (2.3), which is small enough to avoid the overestimation in AF order but still big enough to disallow double occupancy, is important for obtaining solutions that can be considered as approximate solutions of the original t-J model (2.2).

MF-decoupling of (2.3) leads to the MF Hamiltonian[56],

$$\begin{aligned} H^{MF}_{t-J-U} = &- \sum_{i,\delta,\sigma} (t+\tau^{\delta}_{i\sigma}) e^{i\phi^{\delta}_{i}} c^{\dagger}_{i,\sigma} c_{i+\delta,\sigma} - \sum_{i,\sigma} (\mu - \eta_{i\sigma} + \sigma e^{i\mathbf{Q}\cdot\mathbf{r_i}} \sum_{\delta} m_{i,\delta}) n_{i\sigma} \\ &+ \sum_{i,\delta} (\Delta^{\delta}_{i} [c^{\dagger}_{i+\delta,\uparrow} c^{\dagger}_{i,\downarrow} + c^{\dagger}_{i,\uparrow} c^{\dagger}_{i+\delta,\downarrow}] + h.c.) \end{aligned} \tag{2.4}$$

with the self-consistent conditions,

$$\begin{aligned} \Delta^{\delta}_{i} &= \frac{J}{4} (\langle c_{i+\delta\downarrow} c_{i\uparrow} \rangle - \langle c_{i+\delta\uparrow} c_{i\downarrow} \rangle) \\ m_i &= \frac{J}{2} (\langle n_{i\uparrow} \rangle - \langle n_{i\downarrow} \rangle) e^{i\mathbf{Q}\cdot\mathbf{r_i}} \\ \tau^{\delta}_{i\sigma} &= \frac{J}{2} \langle c^{\dagger}_{i+\delta,-\sigma} c_{i-\sigma} \rangle \\ \eta_{i\sigma} &= U \langle n_{i-\sigma} \rangle - \frac{J}{4} \sum_{\delta} \langle n_{i+\delta} \rangle , \end{aligned} \tag{2.5}$$

where $\tau^{\delta}_{i\sigma}$ is the Fock shift, which renormalizes the hopping at site i along direction δ, while $\eta_{i\sigma}$ is the Hartree shift on site i, which renormalizes the local chemical potential. The AF order on site i is represented by m_i, with the sign difference of the local moments between adjacent sites denoted by the exponential term containing the AF ordering vector $\mathbf{Q} = (\pi, \pi)$. Δ^{δ}_{i} is the d-wave SC order defined on the bond between site i and site $i+\delta$.

2.2 UV-model (the extended Hubbard Model)

Variational Monte Carlo calculations on the Hubbard and t-J model have found superconducting solutions with d-wave symmetry[57]. The d-wave SC (dSC) can be studied within mean-field theory using the following effective model,

$$\mathcal{H}_{UV} = -\sum_{i,\delta,\sigma} t_\delta c^\dagger_{i,\sigma} c_{i+\delta,\sigma} - \mu \sum_{i,\sigma} n_{i,\sigma} + U \sum_i n_{i\uparrow} n_{i\downarrow} - V \sum_{i,\delta} n_{i\uparrow} n_{i+\delta\downarrow} \tag{2.6}$$

with $V > 0$ and $U > 0$. Note that in order to study SC within mean-field theory, the effective microscopic Hamiltonian must include an explicit attractive interaction term, and for d-wave SC (dSC), one needs to have an attractive term between nearest-neighbors (nn) sites.[†]

MF-decoupling of (2.6) leads to the MF Hamiltonian,

$$\mathcal{H}^{MF}_{UV} = -\sum_{i,\delta,\sigma} t_{i\delta} c^\dagger_{i,\sigma} c_{i+\delta,\sigma} + \sum_{i,\sigma} (-\mu + \eta_{i\sigma}) n_{i\sigma} + \sum_{i,\delta} \left[\Delta^\delta_i c^\dagger_{i\uparrow} c^\dagger_{i+\delta\downarrow} + h.c. \right], \tag{2.9}$$

with self-consistent conditions,

[†] In t-J model, the nn-attraction necessary for dSC is included in the (AF) Heisenberg interaction as we can see by rearranging it as,

$$H' = \frac{J}{2} \sum_{i,\delta} (\mathbf{S_i} \cdot \mathbf{S_{i+\delta}} - \frac{1}{4} n_i n_{i+\delta}) \tag{2.7}$$

$$= \frac{J}{2} \sum_{i,\delta} \left[S^+_i S^-_{i+\delta} - n_{i\uparrow} n_{i+\delta\downarrow} \right] \tag{2.8}$$

$$\eta_{i\sigma} = U \langle n_{i,-\sigma} \rangle - V \sum_{\delta} \langle n_{i+\delta,-\sigma} \rangle$$
$$\Delta_i^{\delta} = -\frac{V}{2}(\langle c_{i+\delta\downarrow} c_{i\uparrow} \rangle - \langle c_{i+\delta\uparrow} c_{i\downarrow} \rangle). \tag{2.10}$$

This is the main MF model to be studied for the rest of the thesis.

Note that, in general, MF Hamiltonian of a given microscopic Hamiltonian is not unique, and one typically only includes the mean field order parameters of interest in the MF model, while excluding other insignificant mean-fields. For example, in (2.9), some terms with the mean-fields $\langle c_{i\uparrow}^{\dagger} c_{i\downarrow} \rangle$ and $\langle c_{i\uparrow}^{\dagger} c_{i+\delta\downarrow} \rangle$ are not included since such spin-flipping scattering is not present in the absence of local magnetic impurities. In addition, the term with the mean-field $\langle c_{i\downarrow} c_{i\uparrow} \rangle$ is excluded in (2.9) and (2.9), since for the stripe dSC states that we are interested in, such on-site SC pairing has little relevance, and the triplet SC contribution is not considered in (2.9), with the connection to $\mathcal{H}_{t-J-U}^{MF}$ (2.4) in mind, which has no triplet SC channel.

2.3 Connection between tJ-model and UV-model

Comparing $\mathcal{H}_{UV}^{MF}$ (2.9) with $\mathcal{H}_{t-J-U}^{MF}$ (2.4), the mean-field Hamiltonian of the two models are almost identical if one identifies the interaction parameters $\{J,U\} \leftrightarrow \{V,U\}$ in $\mathcal{H}_{t-J-U}^{MF}$ and $\mathcal{H}_{UV}^{MF}$ respectively, except that there is no Fock shift present in $\mathcal{H}_{UV}^{MF}$, which makes no qualitative difference since the effect of Fock shift is simply to renormalize the hopping t. Hence, $\mathcal{H}_{UV}$ and $\mathcal{H}_{t-J-U}$ are qualitatively equivalent at mean field level, and using another connection between $\mathcal{H}_{t-J}$ and $\mathcal{H}_{t-J-U}$ (as established in section 2.1), one can justify that $\mathcal{H}_{UV}$ and $\mathcal{H}_{t-J}$ are qualitatively equivalent at mean field level too. Note that both mean-field

models $\mathcal{H}^{MF}_{t-\hat{J}}$ and H^{MF}_{UV} have a major drawback in that they lack the proper physics necessary for the Mott insulator-to-metal transition, but away from the transition this drawback becomes insignificant and their solutions are physically relevant.

In summary, by solving the UV-model, an effective model that is qualitatively equivalent with the t-J model at mean-field level, we can obtain useful insights on the solutions of the t-J model and hence the physics of cuprate superconductors.

Chapter 3

Numerical Methods

3.1 Bogoliubov-de Gennes calculation

The Bogoliubov-deGennes (BdG) calculation solves the MF Hamiltonian exactly by diagonalizing the Hamiltonian matrix with a unitary transformation called the Bogoliubov transformation. In the following, the formalism for the self-consistent BdG calculation with the UV-model is presented concisely, and further details are given in Appendix A.

For the UV-model, the MF Hamiltonian to solve is given as (2.9) (repeated here for convenience),

$$\mathcal{H}_{UV}^{MF} = -\sum_{i,\delta,\sigma} t_\delta c_{i,\sigma}^\dagger c_{i+\delta,\sigma} + \sum_{i,\sigma}(-\mu+\eta_{i\sigma})n_{i\sigma} + \sum_{i,\delta}\left[\Delta_i^\delta c_{i\uparrow}^\dagger c_{i+\delta\downarrow}^\dagger + h.c.\right], \tag{3.1}$$

with self-consistent conditions,

$$\eta_{i\sigma} = U \langle n_{i,-\sigma} \rangle - V \sum_{\delta} \langle n_{i+\delta,-\sigma} \rangle \tag{3.2}$$

$$\Delta_i^{\delta} = -\frac{V}{2}(\langle c_{i+\delta\downarrow} c_{i\uparrow} \rangle - \langle c_{i+\delta\uparrow} c_{i\downarrow} \rangle), \tag{3.3}$$

which can be diagonalized by a unitary transformation to give:

$$\mathcal{H}_{UV}^{MF} = E_0 + \sum_{n,\sigma} E_{\sigma}^{n} \gamma_{n\sigma}^{\dagger} \gamma_{n\sigma}, \tag{3.4}$$

where E_0 is the ground state energy, $\gamma_{n,\sigma}^{\dagger}$ and $\gamma_{n,\sigma}$ are fermionic quasiparticle creation and annihilation operators respectively for the n-th quasiparticle excitation energy E_{σ}^{n}.

The Bogoliubov transformation, the unitary transformation that diagonalizes (3.1) to give (3.4), has the form,

$$c_{i,\sigma} = \sum_{n} (u_{i,\sigma}^{n} \gamma_{n,\sigma} - \sigma v_{i,\sigma}^{n*} \gamma_{n,-\sigma}^{\dagger}), \tag{3.5}$$

where in order to assure the transformation from (3.1) to (3.4) the coefficients $u_{i,\sigma}^{n}$ and $v_{i,\sigma}^{n}$ must satisfy the following eigenvalue equation, the so-called the BdG equation,

$$\begin{pmatrix} \hat{h} & \hat{\Delta} \\ \hat{\Delta}^* & -\hat{h}^* \end{pmatrix} \begin{pmatrix} \mathbf{u}_{\mathbf{i}\sigma}^{n} \\ \mathbf{v}_{\mathbf{i}-\sigma}^{n} \end{pmatrix} = E_{\sigma}^{n} \begin{pmatrix} \mathbf{u}_{\mathbf{i}\sigma}^{n} \\ \mathbf{v}_{\mathbf{i}-\sigma}^{n} \end{pmatrix}, \tag{3.6}$$

where $\mathbf{u}^n_{\mathbf{i}\sigma} = (u^n_{1\sigma}, u^n_{2\sigma}, \cdots, u^n_{N\sigma})^T$ and the corresponding column vector $\mathbf{v}^n_{\mathbf{i}-\sigma}$ define the wavefunction for the n-th eigenstate with energy $E_{n,\sigma}$, and the operators in the Hamiltonian matrix act on $\mathbf{u}^n_\sigma$ and $\mathbf{v}^n_\sigma$ as,

$$\hat{h}u^n_{i,\sigma} = -\sum_\delta t_\delta u^n_{i+\delta,\sigma} + (-\mu + \eta_{i,\sigma})u^n_{i,\sigma} \tag{3.7}$$

$$\hat{\Delta}v^n_{-\sigma} = \sum_\delta \Delta^s_{i,\delta} v^n_{i+\delta,-\sigma} \tag{3.8}$$

The above equations are written in real space, but for a system with the full lattice symmetry, such as a uniform superconductor, they could equally well be written in momentum space. In this thesis, we are interested in different stripe states mentioned in Chapter 1, all of which are periodic in both x and y direction, and the supercells can be defined in the system according to the translational symmetry of the state, where l_x and l_y define the size of a unit supercell, and M_x and M_y define the number of supercells in the system.

Performing the Fourier transform with respect to the supercells, it can be block-diagonalized as,

$$\begin{pmatrix} \hat{h} & \hat{\Delta} \\ \hat{\Delta}^* & -\hat{h}^* \end{pmatrix} \begin{pmatrix} \mathbf{u}^\mathbf{n}_{\mathbf{i},\sigma}(\mathbf{k}) \\ \mathbf{v}^\mathbf{n}_{\mathbf{i},-\sigma}(\mathbf{k}) \end{pmatrix} = E^n_\sigma(\mathbf{k}) \begin{pmatrix} \mathbf{u}^\mathbf{n}_{\mathbf{i},\sigma}(\mathbf{k}) \\ \mathbf{v}^\mathbf{n}_{\mathbf{i},-\sigma}(\mathbf{k}) \end{pmatrix} \tag{3.9}$$

where $\mathbf{k} = (k_x, k_y) = (\frac{2\pi}{l_x}\frac{m_x}{M_x}, \frac{2\pi}{l_y}\frac{m_y}{M_y})$ with $m_x = 1 \cdots M_x$ and $m_y = 1 \cdots M_y$ is the Bloch wavevector defined in the reduced FBZ [*].

[*] Note that the extra k-dependent phases should be added for the boundary crossing hopping and pairing (the details in Appendixap:bloch)

In summary, the block-diagonalization reduces the original eigenvalue problem defined in real space (3.6), which requires diagonalizing a $2N$ by $2N$ matrix one time, to another eigenvalue problem (3.9), which requires diagonalizing a $2l$ by $2l$ matrices M times ($l = l_x l_y$ is the number of sites in a supercell and $M = M_x M_y$ is the total number of supercells in the system), therefore leading to a significant reduction of computational effort. All the results given in this thesis are produced using this block-diagonalization technique.

3.2 Free Energy

In the BdG calculation, free energy F is given by the well-known Helmholtz expression,

$$F = \langle H \rangle_{MF} - TS, \tag{3.10}$$

where $\langle H \rangle_{MF}$ is the expectation of the microscopic Hamiltonian evaluated with the BdG solutions and S is the system entropy[58].

For the UV-model, the microscopic Hamiltonian is given in (2.6) (repeated here for convenience).

$$\mathcal{H}_{UV} = -\sum_{i,\delta,\sigma} t_{i\delta} c^{\dagger}_{i,\sigma} c_{i+\delta,\sigma} - \mu \sum_{i,\sigma} n_{i,\sigma} + U \sum_{i} n_{i\uparrow} n_{i\downarrow} - V \sum_{i,\delta} n_{i\uparrow} n_{i+\delta\downarrow} \tag{3.11}$$

Applying Wick's theorem to the interaction terms (the subscript $\langle\rangle_{MF}$ is dropped from here on),

$$U\left\langle n_{i\uparrow}n_{i\downarrow}\right\rangle = U\left\langle n_{i\uparrow}\right\rangle\left\langle n_{i\downarrow}\right\rangle \tag{3.12}$$

$$V\left\langle n_{i\uparrow}n_{i+\delta\downarrow}\right\rangle = V\left\langle n_{i\uparrow}\right\rangle\left\langle n_{i+\delta\downarrow}\right\rangle + V\left\langle c^{\dagger}_{i\uparrow}c^{\dagger}_{i+\delta\downarrow}\right\rangle\left\langle c_{i+\delta,\downarrow}c_{i\uparrow}\right\rangle, \tag{3.13}$$

where some terms with mean-fields such as $\langle c_{i\downarrow}c_{i\uparrow}\rangle$, $\langle c^{\dagger}_{i\uparrow}c_{i\downarrow}\rangle$ and $\langle c^{\dagger}_{i\uparrow}c_{i+\delta\downarrow}\rangle$ which do not appear in the mean-field Hamiltonian (2.9) have been dropped on the right sides. Then the internal energy is given as[†],

$$\begin{aligned}\left\langle \mathcal{H}_{UV}\right\rangle = &-\sum_{i,\delta,\sigma} t_{i\delta}\left\langle c^{\dagger}_{i,\sigma}c_{i+\delta,\sigma}\right\rangle - \mu\sum_{i,\sigma}\left\langle n_{i,\sigma}\right\rangle + U\sum_{i}\left\langle n_{i\uparrow}\right\rangle\left\langle n_{i\downarrow}\right\rangle \\ &- V\sum_{i,\delta}\left(\left\langle n_{i\uparrow}\right\rangle\left\langle n_{i+\delta\downarrow}\right\rangle + \left\langle c^{\dagger}_{i\uparrow}c^{\dagger}_{i+\delta\downarrow}\right\rangle\left\langle c_{i+\delta,\downarrow}c_{i\uparrow}\right\rangle\right).\end{aligned} \tag{3.14}$$

The entropy S, which in the BdG construction is the entropy of the system of non-interacting fermionic quasiparticles, is calculated as,

$$S = -\sum_{n,\sigma}\left[f_{n,\sigma}\ln f_{n,\sigma} + (1-f_{n,\sigma})\ln(1-f_{n,\sigma})\right], \tag{3.15}$$

where $f_{n,\sigma} = \frac{1}{1+e^{\beta E^{n}_{\sigma}}}$ is the usual Fermi function with the quasiparticle energy, E^{n}_{σ}.

In summary, using (3.14) and (3.15), the free energy is calculated as in (3.10). Note that all the free energy results presented in this thesis are given in terms of free energy density (average free energy per site).

[†] With the block-diagonalization, the summation is only over the sites in a unit supercell, and the free energy density is obtained by dividing the resulting free energy by the number of sites in a unit supercell

3.3 Density of States (DOS) and Spectral Weight Function

Based on the quasiparticle wave functions $\Psi^n_\sigma = (\mathbf{u}^n_\sigma, \mathbf{v}^n_{-\sigma})$ $(n = 1 \cdots N)$, the Local Density of States (LDOS) at site i is calculated as,

$$LDOS(i,E) = \sum_{n=1,\sigma}^{N} \left[|u^n_{i,\sigma}|^2 \delta(E - E^n_\sigma) + |v^n_{i,\sigma}|^2 \delta(E + E^n_\sigma) \right], \tag{3.16}$$

where N is the total number of lattice sites in the system.

The spectral weight function is calculated as, using the Fourier transformed quasiparticle wavefunctions given in k-space,

$$A(\mathbf{q},E) = \sum_{n=1,\sigma}^{N} \left[|u^n_\sigma(\mathbf{q})1^2 \delta(E - E^n_\sigma) + |v^n_\sigma(\mathbf{q})|^2 \delta(E + E^n_\sigma) \right], \tag{3.17}$$

For the case where there are $l = l_x l_y$ sites per supercell, the LDOS at site i can be written as,

$$LDOS(i,E) = \frac{1}{M} \sum_{\mathbf{k},\sigma} \sum_{n=1}^{l} \left[|u^n_i(\mathbf{k})|^2 \delta(E - E_n) + |v^n_i(\mathbf{k})|^2 \delta(E + E_n) \right], \tag{3.18}$$

where $M = M_x M_y$ is the number of super cells defined in the system which is equal to the number of k-points defined in the reduced BZ, and the spectral weight function can be calculated

as in (3.17), although the wavefunction defined in the reduced BZ first needs to be converted to the one defined in the original BZ. ‡

The average Density of States per site (DOS) is calculated by averaging the LDOS over all sites,

$$DOS(E) = \frac{1}{N}\sum_i LDOS(i,E) \tag{3.19}$$

where N is the number of sites to be traced over.

‡ One way to obtain the wavefunctions in the original BZ is to first perform a Fourier transform to reconstruct the real space wavefunctions, then perform another a Fourier transform to go from the full real space to full k-space, i.e.,

$$u_i^n(\mathbf{k}) \xrightarrow{FT} u_i^n(\mathbf{R}) = u^n(\mathbf{r}) \xrightarrow{FT} u^n(\mathbf{q})$$

Chapter 4

Results (Non-self-consistent)

In this chapter, the nature of the Fermi surface for stripe states is studied by means of a non-self-consistent BdG calculation. One result of self-consistency (studied in the next chapter) is that a PDW state is only stable with sufficiently large interactions. Here, with non-self-consistent results, we can study weaker interactions that leave parts of the original Fermi surface intact in the PDW state.

4.1 Method

A simple effective MF model for stripe SC states with coexisting PDW, CDW and SDW order is given as,

$$\mathcal{H}^{MF} = -\sum_{i,\delta,\sigma} t_\delta c^\dagger_{i,\sigma} c_{i+\delta,\sigma} - \mu \sum_{i,\sigma} n_{i\sigma} + \sum_{i,\sigma} \eta_{i\sigma} n_{i\sigma} \tag{4.1}$$

$$+ \sum_i \Delta \left\{ \cos\left[Q_x (x - \frac{1}{2})\right] \left[c^\dagger_{i\uparrow} c^\dagger_{i+\hat{x}\downarrow} + c^\dagger_{i+\hat{x}\uparrow} c^\dagger_{i\downarrow} \right] - \cos\left(Q_x i_x\right) \left[c^\dagger_{i\uparrow} c^\dagger_{i+\hat{y}\downarrow} + c^\dagger_{i+\hat{y}\uparrow} c^\dagger_{i\downarrow} \right] + h.c. \right\}, \tag{4.2}$$

with

$$\eta_{i\sigma} = V_C \cos\left[2Q_x(i_x+1)\right] + sign(\sigma)V_S(-1)^{(i_x+i_y)} \sin\left(Q_x i_x\right) \tag{4.3}$$

where $sign(\sigma) = \pm 1$ for $\sigma = \{\uparrow,\downarrow\}$, and (Δ, V_C, V_S) are the mean fields which drive PDW, CDW, and SDW order respectively, and all the wave vectors and respective phases are chosen to give typical coexisting stripe SC solutions as shown in Fig. 4.1. The resulting non-self-consistent solutions upon a diagonalization * can be used to calculate the resulting charge, spin and pair density on each site as,

$$n_i = \langle n_{i\uparrow}\rangle + \langle n_{i\downarrow}\rangle \tag{4.4}$$

$$m_i = \langle n_{i\uparrow}\rangle - \langle n_{i\downarrow}\rangle \tag{4.5}$$

$$P_i^{\delta} = \frac{\langle c_{i+\delta\downarrow} c_{i\uparrow}\rangle - \langle c_{i+\delta\uparrow} c_{i\downarrow}\rangle}{2} \tag{4.6}$$

and the magnitude of each density wave is given as,

$$\triangle n = \frac{\max(n_i) - \min(n_i)}{2} \tag{4.7}$$

$$\triangle m = \frac{\max(m_i) - \min(m_i)}{2} \tag{4.8}$$

$$\triangle P = \frac{\max(|P_i^d|) - \min(|P_i^d|)}{2} \tag{4.9}$$

$$\tag{4.10}$$

* block-diagonalization as discussed in Chapter 3. The super cell size is set based on which order(s) exist, i.e. $(l_x, l_y) = (8,2)$ by default, and $(l_x, l_y) = (8,1)$ without SDW, and $(lx, ly) = (4,1)$ with only CDW.

with

$$P_i^d = \frac{1}{4}(P_i^{\hat{x}} + P_i^{-\hat{x}} - P_i^{\hat{y}} - P_i^{-\hat{y}}). \tag{4.11}$$

Note that, in general, the calculated spin, charge and pair densities will not follow the simple sinusoidal spatial dependence of the mean fields because the density of states (in the absence of order) is not a constant away from the bottom or top of the band, and it usually requires the Fourier transform with the first few harmonics of the natural wave vector to fully describe the density waves. Here, the resulting solutions are found to take almost sinusoidal forms, hence the real space configuration of non-self-consistent stripe solutions can be characterized conveniently by a set of parameters $(\rho, \triangle P, \triangle n, \triangle m)$. This is demonstrated in Fig. 4.1 with a typical non-self-consistent PDW solution as an example, where the corresponding spectral weight function at the Fermi level and Fermi Surface (FS) are also shown.

4.2 Results

All the results given in this Chapter are produced with the same band parameters $(t, t', \mu) = (1, -0.4, -1.14)$, which give the target filling $\rho = 0.875$ for the non-interacting case. The temperature is $T = 0.01t$, and the lattice size is $(N_x, N_y) = (320, 320)$ to obtain enough resolution for the plots given in k-space.

Fig. 4.2 shows the spectral weight and FS of the PDW solutions obtained with varying input parameters (Δ, V_c) but with fixed $V_s = 0$, in order to study the simplest case with co-existing PDW and CDW order without SDW order, one likely scenario in stripe SC states. Fermi arcs near the nodal points resulting from open orbits are observed for the states with relatively weak PDW and CDW, but as PDW order becomes strong, the FS is reconstructed to

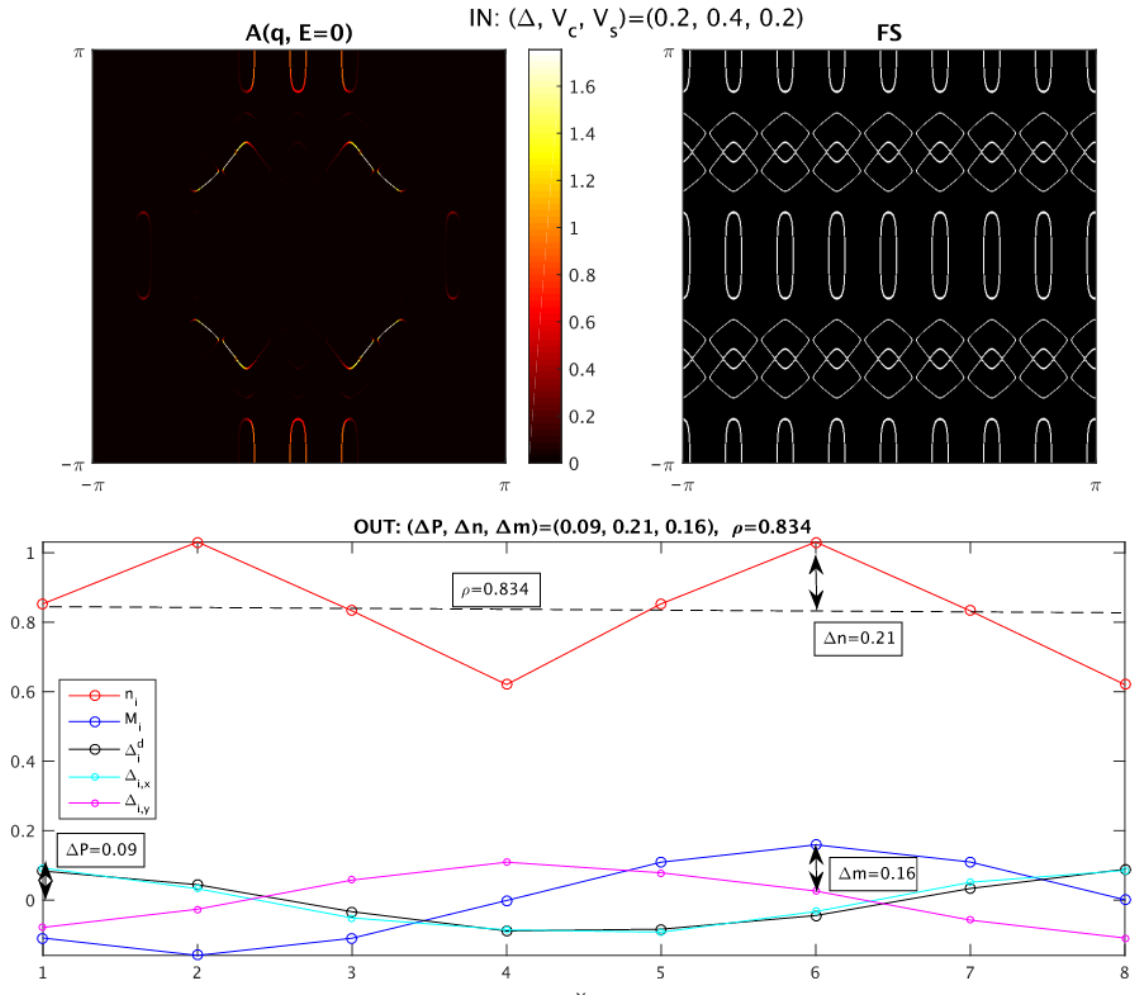

Figure 4.1: A typical non-self-consistent PDW solution obtained with a set of input parameters $(\Delta, V_c, V_s) = (0.2, 0.4, 0.2)$. (Bottom) the real space configuration characterized with a set of order parameters $(\triangle P, \triangle n, \triangle m) = (0.09, 0.21, 0.16)$ shown in a unit supercell. (Top) (Left) the spectral weight function at the Fermi level $A(\mathbf{q}, E = 0)$ in BZ, and (Right) Fermi Surface in the extended zone scheme.

form small pockets. Note that these pockets cannot be characterized as either hole or electron pockets, since quasiparticles which form the FS are superposition of both particles and holes. Instead, the pockets are characterized as "hole-like", which can be most directly seen in the occupation number plot $n(\mathbf{k})$, where the occupation number inside of the pockets are close to zero[59].

Fig. 4.3 shows the spectral weight and FS of the PDW solutions obtained with varying input parameters (V_c, V_s) but with fixed $\Delta = 0.2$, in order to study the effect of CDW and SDW on stripe SC states. The first thing to notice in this figure is that SDW order is mostly responsible for the reconstructions of FS, and the spectrum is completely gapped for $\Delta_{SDW} \geq 0.4$, while CDW order is found to have little qualitative effect over the parameter range studied. Although the arc-like structures are also seen in the finite SDW cases obtained with $V_s = 0.4$, this arc is qualitatively different in that the arc is actually one side of small hole-like pockets in anti-nodal regions where the other side with small spectral weight is not seen, another likely scenario especially in ARPES measurements.

Another important thing to note is that the magnitude of SDW order has little effect on that of PDW order, therefore both orders can coexist. This is actually reflected in the model itself, where the two potentials to drive SDW and PDW order are out of phase to each other. Kampf et.al. gave another description of coexisting SDW and PDW order by calculating the correlation function for both orders, $P^2(\mathbf{k}) = \sum_{\mathbf{q}} \langle c_{-\mathbf{k}+\mathbf{q}} \downarrow c_{\mathbf{k}\uparrow} \rangle^2$ and $\rho_s = \sum_{\mathbf{q}} \sum_s \langle s c^\dagger_{\mathbf{k}+\mathbf{q}s} c_{\mathbf{k}s} \rangle$, with the self-consistent PDW solutions obtained with the U-model, which suggests that SDW correlation mostly lives along the diagonal parts of FS connected by AF wave vector $Q_{AF} = (\pi, \pi)$, while PDW correlation lives in anti-nodal regions (Kampf et.al., 2011).

Fig. 4.4 is analogous to Fig. 4.3 but with PDW order turned off by setting $\Delta = 0$. Comparing Fig. 4.4 with Fig. 4.3, one can conclude that the anti-nodal regions are gapped out by

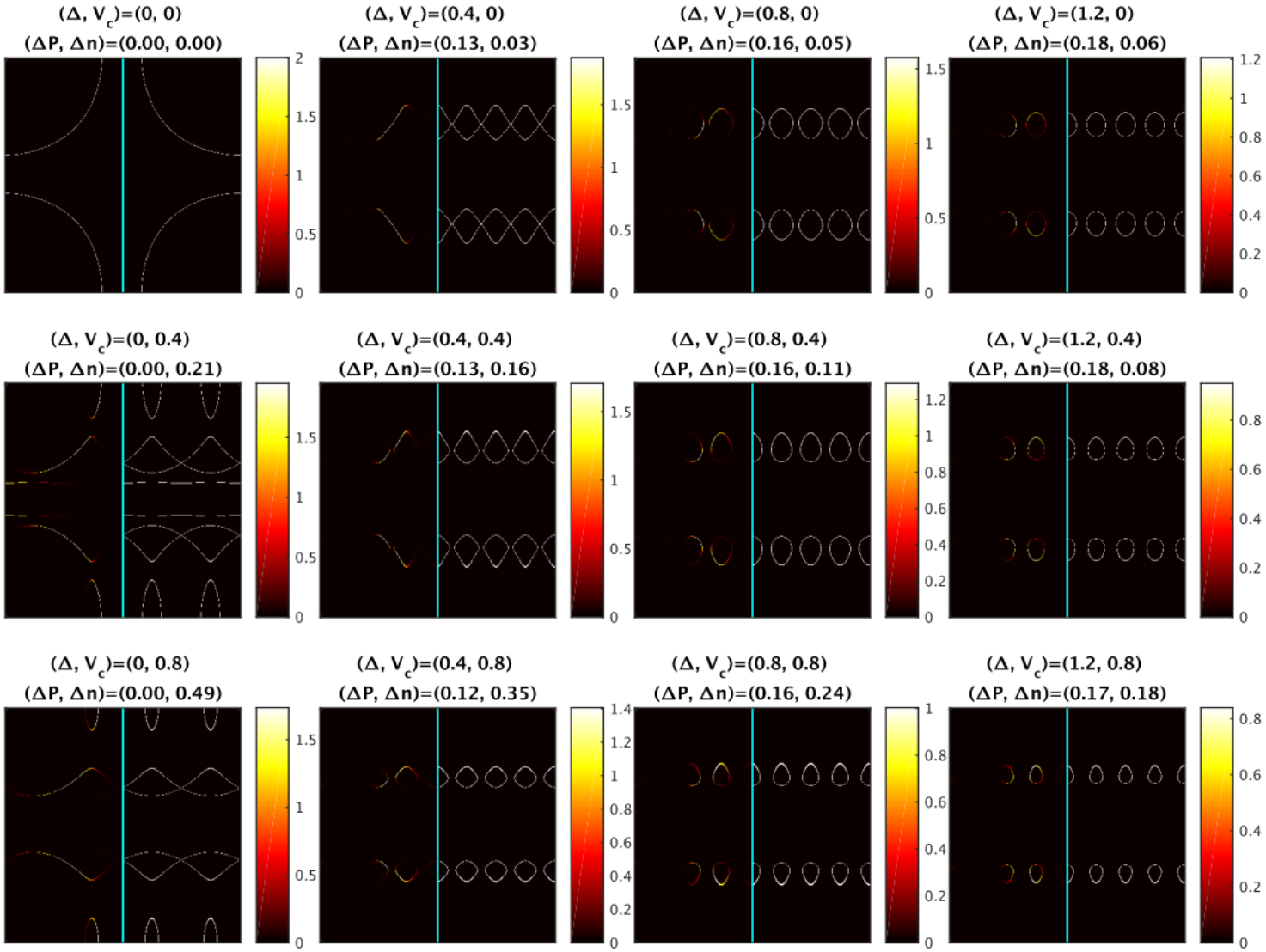

Figure 4.2: Spectral weight function at the Fermi level $A(\mathbf{q}, E = 0)$ and the Fermi Surface of non-self-consistent PDW solutions with different sets of input parameters (Δ_d, V_c) with fixed $V_s = 0$, hence no SDW order ($\triangle m = 0$) for all the solutions shown here. Spectral weight is plotted on the left half of FBZ, and FS is plotted on the right half for each solution. The colorbar is applicable only for spectral weight (left half). The fixed chemical potential $\mu = -1.14$ is used for all, which gives the target filling $\rho = 0.875$ for the non-interacting case $(\Delta, V_c, V_d) = (0, 0, 0)$ and $\rho = 0.84 \sim 0.87$ for the other interacting cases.

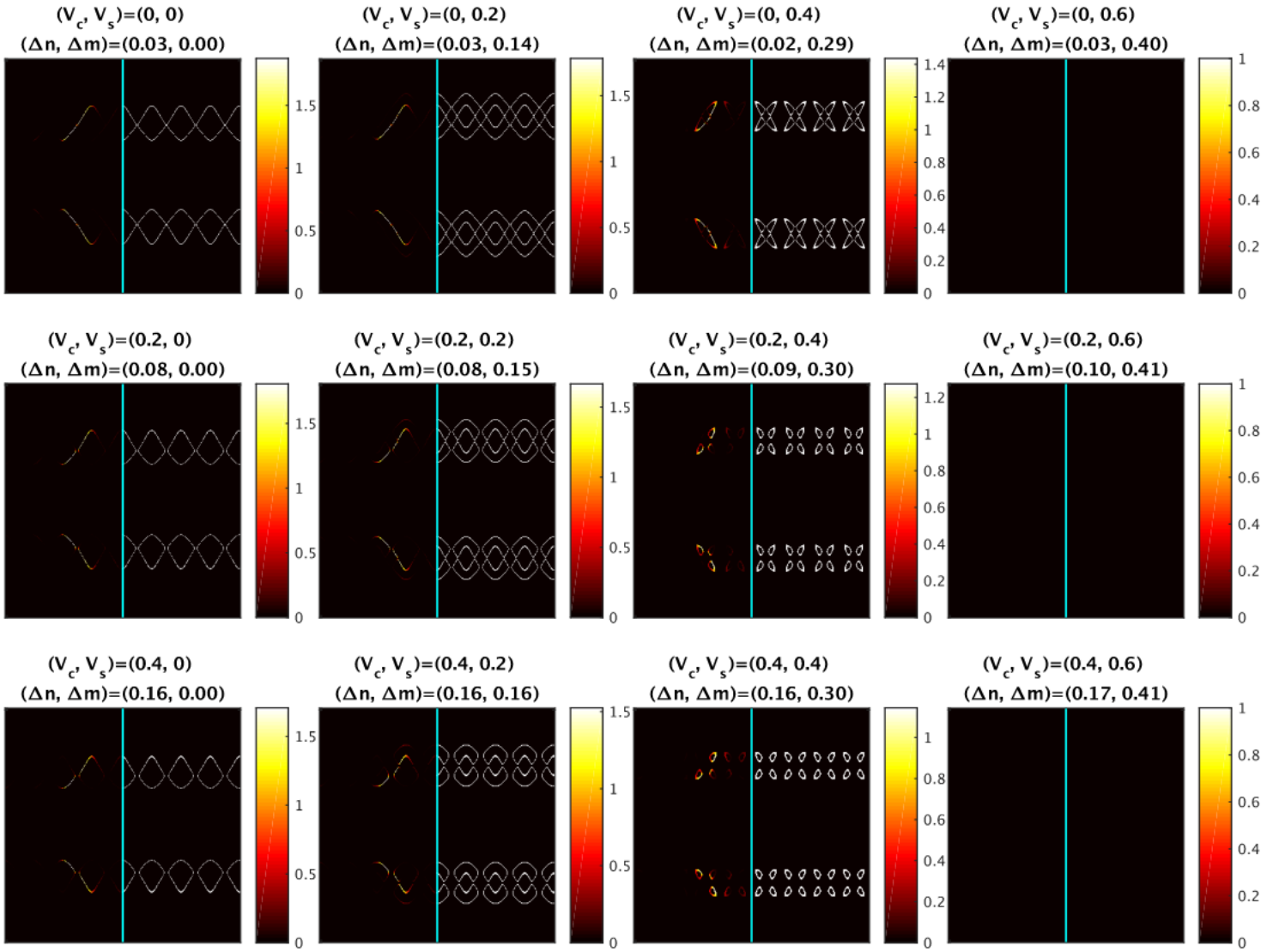

Figure 4.3: varying (V_c, V_s) with fixed $\Delta = 0.4$, which gives $\Delta_{PDW} = 0.126 \sim 0.134$ for the solutions shown here.

PDW order. The fact that SDW is mostly responsible for FS reconstruction is also confirmed at strong CDW with weak SDW limit in Fig. 4.5, although this limit is not a physical regime for cuprates since some sites are more than half-filled.

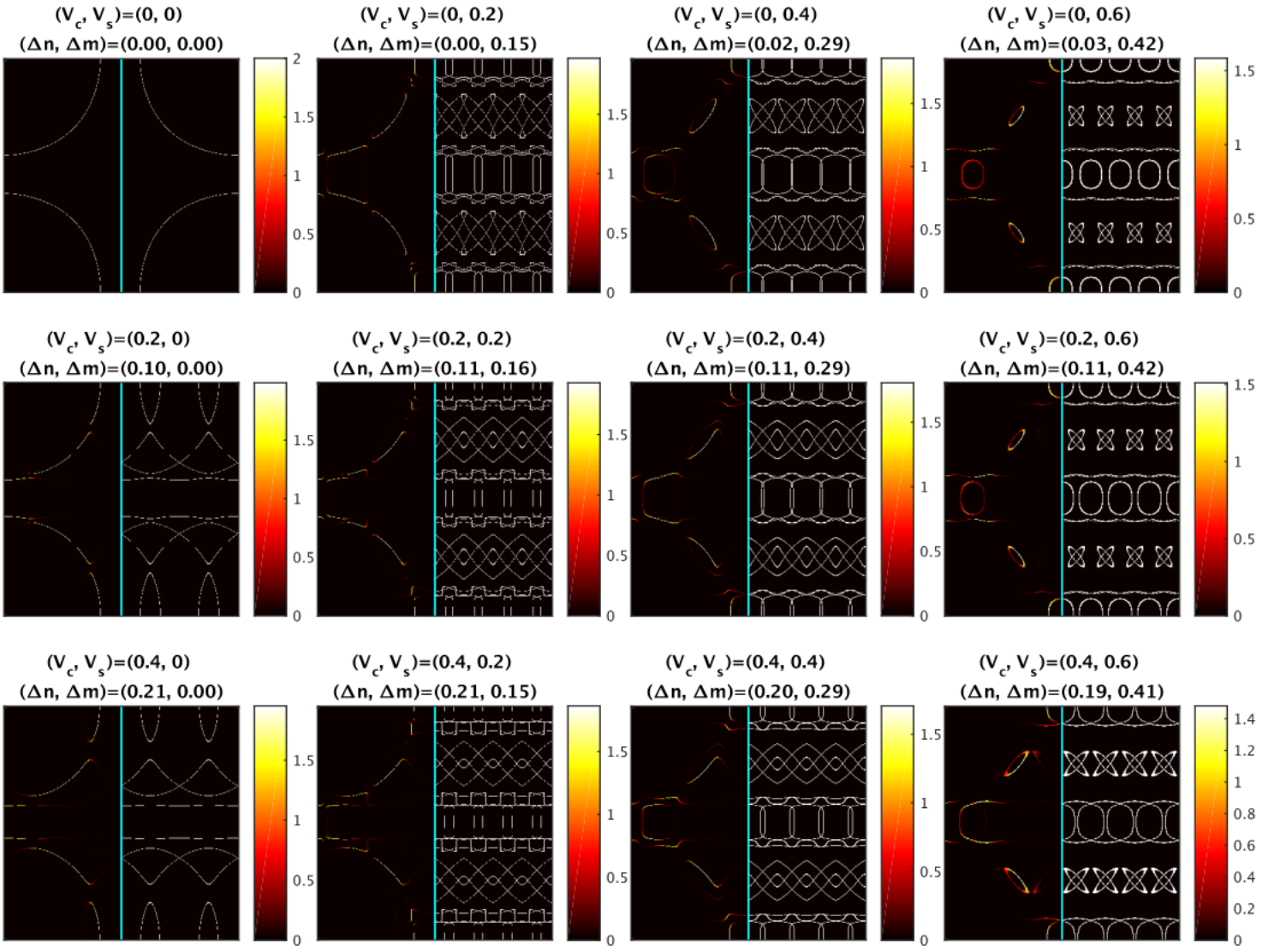

Figure 4.4: analogous to Fig. 4.3, but with PDW turned off by setting $\Delta = 0$.

The effect of SDW order on FS reconstruction is further studied in Fig. 4.6, where V_s is the only variable with fixed $(\Delta, V_c) = (0, 0.2)$. The top left plot corresponds to pure CDW state,

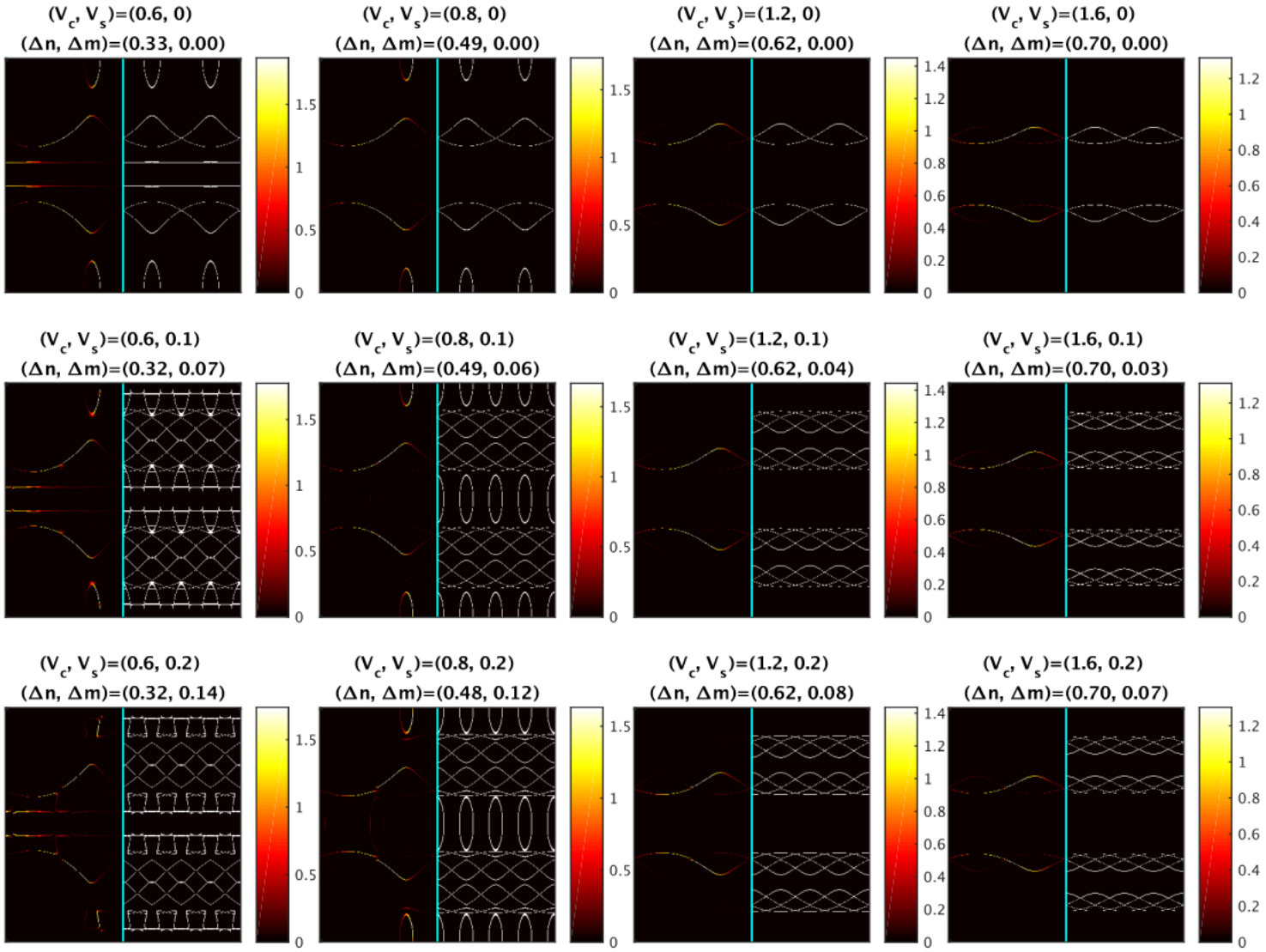

Figure 4.5: analogous to Fig. 4.4 (no PDW) but at strong CDW with weak SDW limit.

where the spectrum shows a signature of CDW gap at parts of FS which can be connected by the wave vector $2\mathbf{Q_x} = (\pi/2, 0)$. As SDW order increases with increasing V_s, further gaps are introduced at parts of FS which can be connected by AF and SDW wave vector, $Q_{AF} = (\pi, \pi)$ and $\mathbf{Q_x} = (\pi/4, 0)$. In the bottom left plot, the FS is similar to that of uniform AF order, where small hole pockets and electron pockets exist at nodal and anti-nodal regions respectively, and

the difference in FS can be understood as the effect of CDW and SDW order. Then once the magnitude of SDW order exceeds a certain limit, the FS becomes 1D like, where the Fermi velocity is in the y direction, hence corresponding to a 1D metal. This 1D metal/SC behavior is also found in all the self-consistent stripe solutions discussed in the next chapter, all of which come with strong SDW order.

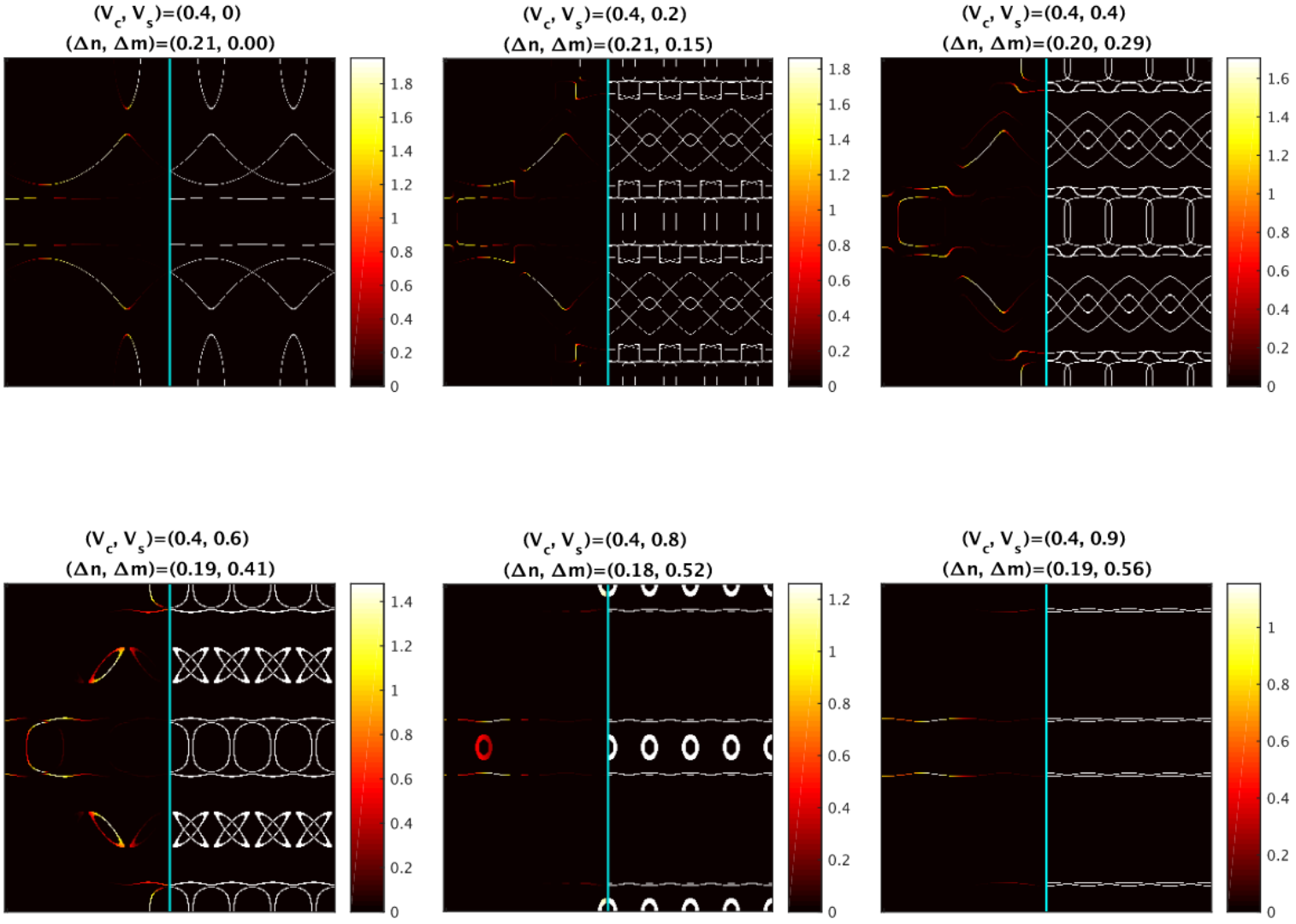

Figure 4.6: analogous to Fig. 4.4, but with fixed $(\Delta, V_c) = (0, 0.4)$, in order to study the effect of SDW on the FS reconstruction specifically.

Overall, in the non-self-consistent calculations for stripe SC states carried out in this section, the Fermi Arcs are observed most vividly in the solutions with PDW and CDW but without SDW order, which is suggested to be the physical regime, both theoretically and experimentally. While the Fermi arcs may exist with small coexisting SDW order as discussed, all the self-consistent solutions found in the next chapter have strong SDW and the FS is fully gapped, which casts some doubt on the applicability of the models used or the mean field approach itself. Another interesting finding is that SDW order or AF stripe can produce a rich FS structure due to the symmetry breaking and nesting based on the two associated vectors $Q_{AF} = (\pi, \pi)$ and $Q_{SDW} = (2\pi/l_x, 0)$, which might play an important role in the mechanism of superconductivity in cuprates.

Chapter 5

Results (self-consistent)

In this chapter, the results of self-consistent BdG calcualtions with the UV-model are presented. The BdG equations used in this chapter are given by (2.9), and the self-consistency conditions are given by (2.10) for the UV-model, where the Hartree shift contribution from V term is set to be zero for the U-model[49].

In section 5.1, the physical properties of PDW solutions obtained with two models, the UV-model and U-model, are discussed. In section 5.2, the stability of various self-consistent stripe SC solutions is investigated with varying input parameters in the model, which leads to a good understanding of the parameter regions where the stripe SC states are stabilized.

Note that in this chapter, all the solutions are self-consistent unless otherwise mentioned (e.g., when they are compared to the non-self-consistent solutions), the fixed band parameters $(t,t') = (1,-0.4)$ are used to give a realistic FS for cuprates, and all the values of interactions and other energies are given in the unit defined by nearest-neighbor hopping parameter $t = 1$. The details of the implementation, such as the convergence criteria and a method to adjust the chemical potential to achieve the target filling, are given in Appendix A (and a sample pseudocode which demonstrates the flow of calculations is given in Appendix B).

5.1 Physical properties of PDW solutions

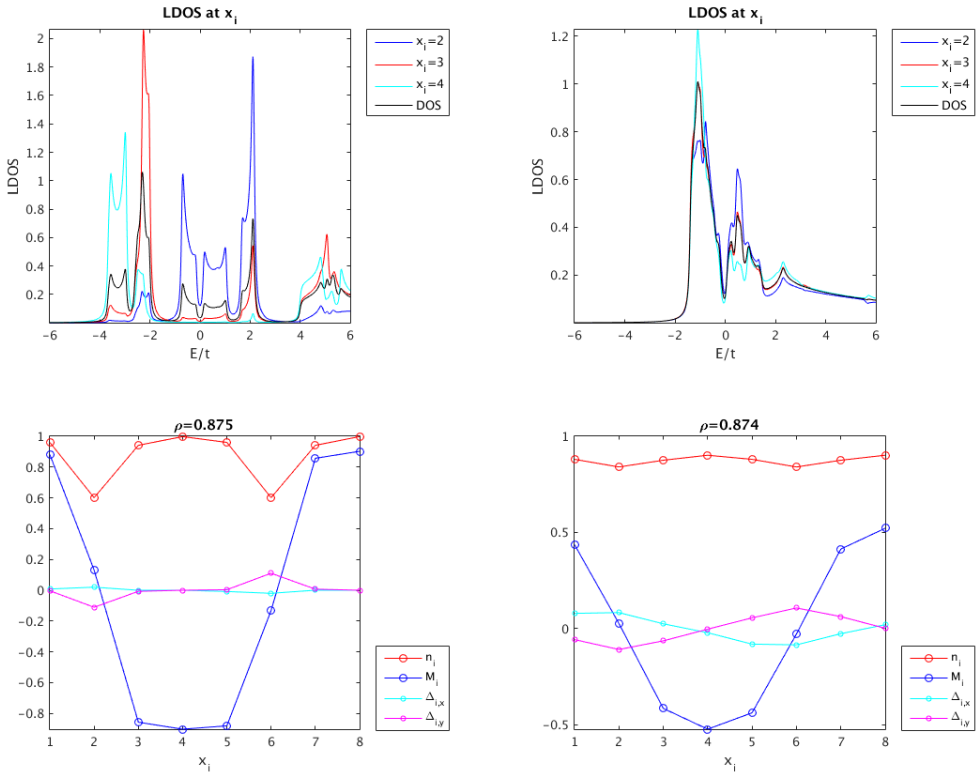

Figure 5.1: LDOS plots for self-consistent PDW solutions obtained with (Left) UV model and (Right) U model with $(U,V) = (3,1.5)$. The definitions of n_i, M_i, $\Delta_{i,x}$ and $\Delta_{i,y}$ are the same as in Chapter 4. For both solutions, the Fermi surface is entirely gapped out, hence the plots of their spectral weight function at the Fermi level and the Fermi Surface are not shown here. Note that $DOS(E=0) \neq 0$ is a numerical artifact due to the finite width of the energy window $\delta E = 0.01t$ used.

Fig. 5.1 shows the real space configuration and Local Density of States (LDOS) of PDW solutions obtained with two different MF models, the UV model given in (2.9) and U model. Both solutions are obtained with the same parameters $(U,V) = (3,1.5)$ at $(\rho,T) = (0.875,0.01)$.

The generic properties of a PDW solution obtained with UV-model are as follows. The system is separated into (a) hole-rich, non-magnetic, close to quarter filled ($\rho = 0.5$) SC re-

gions (b) almost half-filled ($\rho = 1$), three-legged AF regions. SC order is suppressed in the AF region and vice versa, due to the competition between SC and AF order. SC order also shows a directional dependence, where the significant SC order parameters exist only along the vertical non-magnetic lines, i.e. the system shows a quasi-1D SC behavior along the vertical non-magnetic lines. This can be understood as a Non-SC stripe state, which was quasi-1D metallic along the vertical lines and insulating in AF regions, making a SC transition at low temperature.

Compared to the PDW solutions of the UV-model, those of the U-model come with smaller CDW and SDW, and the SC order parameter is more isotropic, less one-dimensional. This is because, while in UV-model, the spins in AF region are almost fully polarized to give a strong AF order and the phase separation between SC and AF regions is strong, hence SC is mostly along non-magnetic vertical lines, in the U model, the weaker AF order due to the smaller Hartree shift allows some SC to exist in AF region and hence the system shows more 2D-like SC behavior. This PDW solution obtained with U-model is qualitatively equivalent to the non-self-consistent PDW solutions with strong SDW order studied in chapter 4, where the original FS without PDW has a 1D FS, hence showing a 1D metal behavior but the resulting PDW order still extends beyond the 1D metallic stripes, resulting in more 2D-like behavior. The 2D nature of superconductivity in the PDW solution of the U-model was additionally confirmed by observing an oscillating behavior in the effective hopping amplitude $\rho_C(\mathbf{r_i}) = \sum_s \langle c^\dagger_{0s} c_{is} \rangle$ and pairing amplitude $P(\mathbf{r_i}) = \langle c_{0\downarrow} c_{i\uparrow} \rangle$ in both x and y directions[49].

The qualitative difference between PDW solutions of the two different models is also clearly seen in the LDOS plots shown in Fig. 5.1. For the PDW solution in the UV-model, the LDOS varies significantly over different sites and the low energy excitation near the Fermi

level is predominantly from the SC site ($x_i = 2$), while for the PDW solution in the U-model, the LDOS does not have any significant site dependence.

In summary, both UV and U model support the PDW solutions self-consistently, although the nature of these PDW solutions vary, namely the nature of superconductivity being 1D-like and 2D-like in the UV and U model respectively. However, the interactions strong enough to stabilize PDW solutions inevitably lead to the strong SDW order in both PDW solutions, making the underlying FS 1D-like as seen in the non-self-consistent solutions with strong SDW order in Chapter 4. This leads to the completely gapped FS upon introducing PDW order.

5.2 Stability of stripe SC states

In this section, the stability of various SC states is studied with varying parameter sets (U,V,ρ,T). The (U,V) dependence of stability of PDW solutions is studied first with fixed $T = 0.01$ in section 5.2.1 in order to determine the physically relevant parameter region (U,V,ρ) for the PDW states, and then the ρ and T dependence of various stripe SC states is studied in detail for a set of parameters (U,V) in section 5.2.2.1 and 5.2.2.2.

For the rest of this thesis, the SC and PDW order parameters are defined as*,

$$\Delta_{SC} = average(\Delta_i^d) \tag{5.1}$$

$$\Delta_{PDW} = max(\Delta_i^d) - \Delta_{SC}, \tag{5.2}$$

where the d-wave SC pairing at a site Δ_i^d is given as,

$$\Delta_i^d = \frac{1}{4}(\Delta_i^{\hat{x}} + \Delta_i^{-\hat{x}} - \Delta_i^{\hat{y}} - \Delta_i^{-\hat{y}}). \tag{5.3}$$

In addition, in order to characterize the directional dependence or the effective "dimensionality" of SC found in stripe SC solutions, a new parameter d_{xy} is used, which is defined as,

$$d_{xy} = 1 + \frac{max(|\Delta_i^{\hat{x}}|)}{max(|\Delta_i^{\hat{y}}|)}, \tag{5.4}$$

* Note that the SC paring Δ_i^δ is generally a complex number, but in the absence of magnetic field, if one sets all the initial Δ_i^δ to be real, all the converged Δ_i^δ after the self-consistent iterations are also real.

where the maximum is taken over sites i and the ratio of the maximum magnitude of SC order parameter in x and y direction approaches 1 if SC in the system is isotropic, hence giving $d_{xy} = 2$, while the ratio approaches 0 if the system has quasi-1D SC behavior, hence giving $d_{xy} = 1$.

The specific heat at a given temperature is calculated based on entropy S[58],

$$C_V(T = T_n) = T_n \frac{dS(T_n)}{dT_n} \simeq T_n \frac{S(T_{n+1}) - S(T_n)}{T_{n+1} - T_n} \tag{5.5}$$

where the entropy at two neighboring temperatures $(T_n < T_{n+1})$ are used, hence it is not calculated for the calculations with fixed T.

5.2.1 (U,V) dependence

Fig. 5.2 shows the filling dependence of the PDW order parameter Δ_{PDW} of PDW solutions obtained with UV model with varying interactions at constant $T = 0.01$, as well as the magnitude of concomitant CDW and SDW order. The main finding here is that the magnitude of the PDW order parameter Δ_{PDW} is almost solely dependent on V. The filling or doping range where PDW states are stabilized is mostly dependent on the band parameter (t,t') used and how well the resulting FS at a given filling is nested by the stripe wave vector $\mathbf{Q_x} = (2\pi/l_x, 0) = (\pi/4, 0)$, consequently showing a complimentary dependence on the interaction strength (U,V), since strong interactions allow the nesting to happen more easily even at parts of FS not exactly nested.

In general, the magnitudes of CDW and SDW monotonically increase as U and V increase, since both U and V scale the magnitude of the Hartree shift and hence of inhomogeneity, but

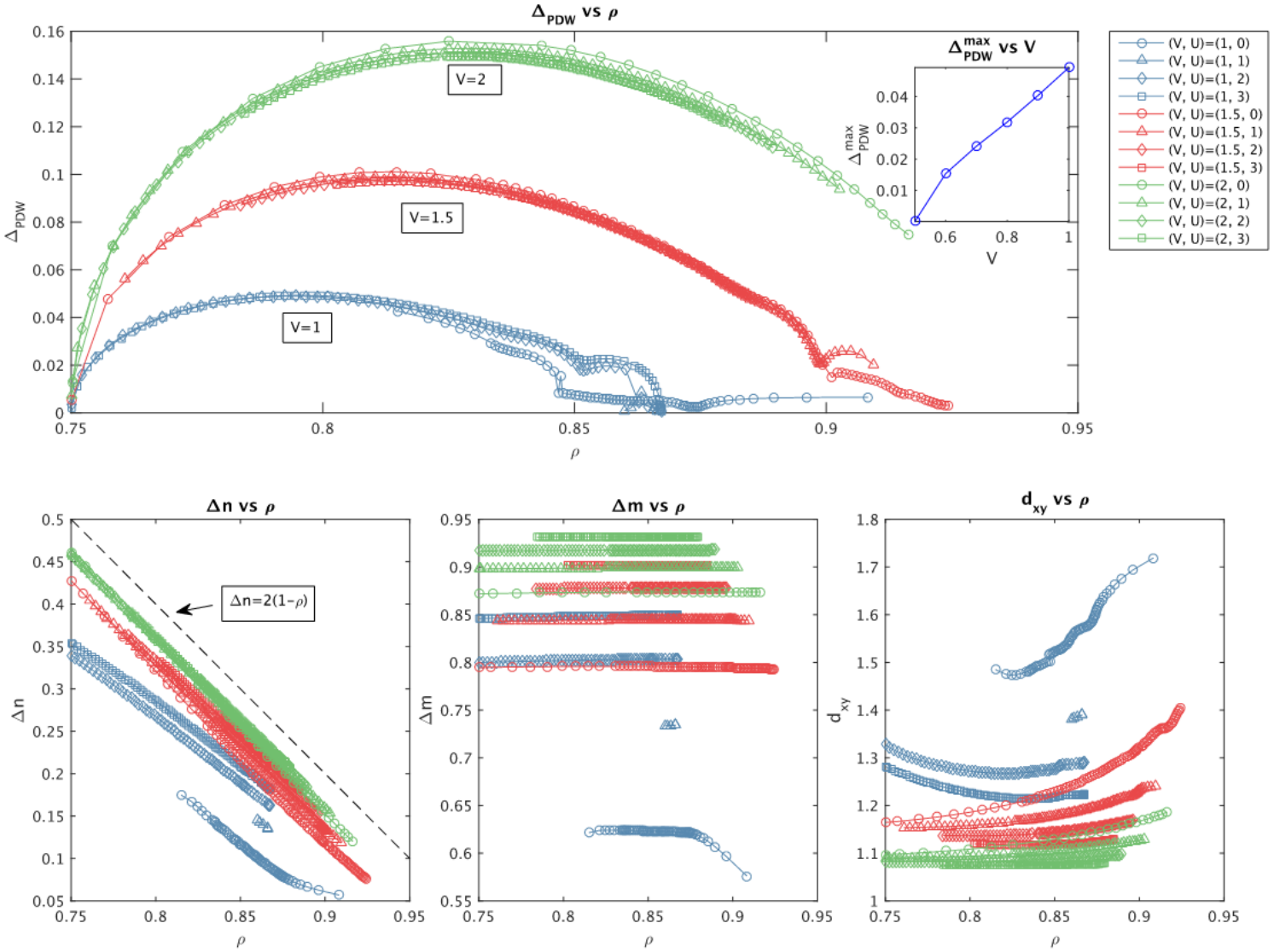

Figure 5.2: The (U, V, ρ) dependence of (Top) the PDW order parameter Δ_{PDW}, (Bottom) the magnitude of CDW and SDW, $\triangle n$ and $\triangle m$, and the effective dimensionality of SC, d_{xy}, for the PDW solutions in the UV-model. The inset in the Δ_{PDW}-ρ plot shows the V dependence of the maximum PDW order parameter at small V limit ($V = 0.5 \sim 1$ with fixed $U = 3$), which occurs near $\rho = 0.78 \sim 0.8$. The dashed line shown in the $\triangle n$-ρ plot corresponds to a scenario where all the holes go into the hole-rich regions with half-filled AF regions. Data points for each state terminate where the states become unstable and the convergence is not achieved. The peculiar behavior observed at the tails of some curves toward the upper cut off in ρ are due to either finite size effects or change in domain structures, which are further discussed in the text.

for the parameter region investigated, the effect of V is more dominant. For the CDW order, the filling sets an upper-bound on the magnitude of modulation. At a given filling ρ, the maximum amplitude of CDW $\triangle n$ is achieved if all the holes go into the hole-rich SC regions and all the AF sites are half-filled (i.e. $\langle n_i \rangle$=4ρ − 3 for a SC site, $\langle n_i \rangle = 1$ for three AF sites) , which gives $\triangle n = 2(1-\rho)$. Strong interaction approaches this limit, but the linear dependence of $\triangle n$ on ρ is found to be generic for all sets of (U,V) investigated. For the SDW order, $\triangle m$ corresponds to the magnetization at the center of AF region, where it is almost half filled, and the spin at that site can be fully polarized in the strong interaction limit.

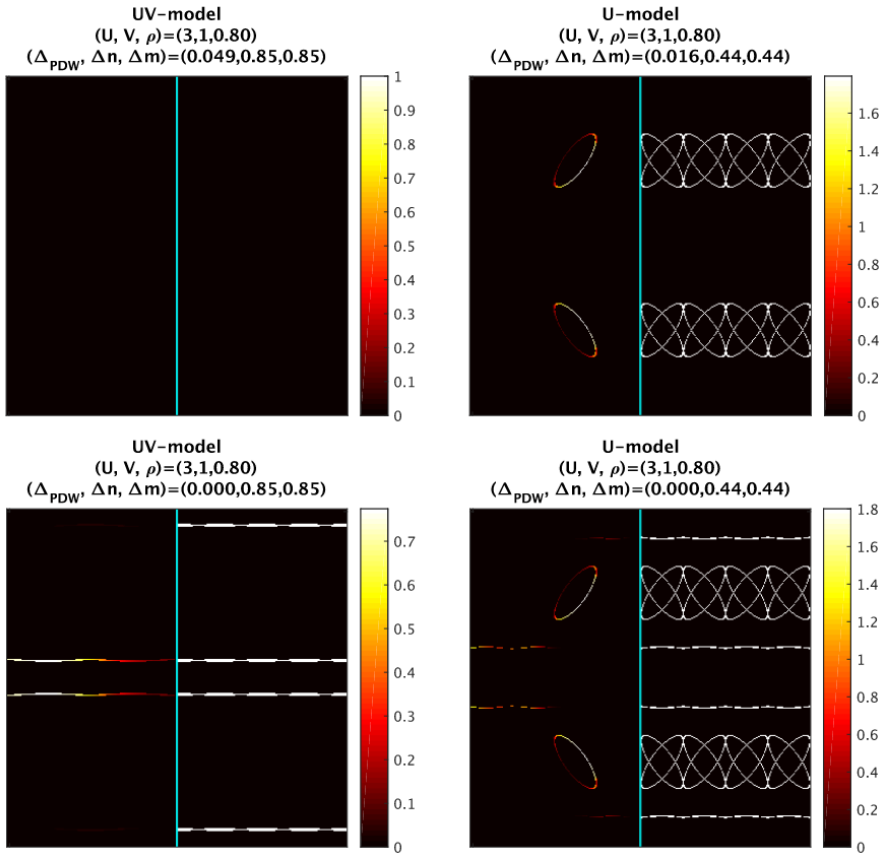

Figure 5.3: Spectral weight function at the Fermi level and the FS for PDW solutions obtained at $(U,V,\rho) = (3,1,0.8)$ with (Top Left) UV-model and (Top Right) U-model. (Bottom) the underlying Fermi Surface for the corresponding non-SC stripe states.

Fig. 5.3 shows the spectral weight function at the Fermi level and the FS for the PDW solutions obtained with the UV-model and U-model at the same parameters $(U,V,\rho) = (3,1,0.8)$, and the underlying FS is also investigated by setting the PDW order to be zero in each solution. For the PDW solutions of the UV-model, the spectrum is completely gapped out with the PDW order, and the underlying FS is 1D-like due to the strong SDW order present, while for the PDW solutions of the U-model, the hole-like pockets are observed at the nodal regions, and the underlying FS without PDW order additionally has a 1D-like FS at antinodal regions, which is gapped out by PDW order. Note that these hole-like pockets are the consequence of the relatively weak SDW order, and hence they get destroyed once strong enough SDW order sets in, and the FS becomes 1D-like as in the PDW solution of the UV-model.

5.2.2 (ρ, T) dependence

In this section, the filling ρ and temperature T dependence of stripe SC states are studied with a set of parameter $(U,V) = (3.5,1.5)$. Although the stripe SC solutions can be stabilized with smaller $V \leq 1$ in more physical regime as discussed in section 5.2.1, the stabilization is possible only near the optimal doping at lowest T. This corresponds to small PDW order parameter $\Delta_{PDW} < 0.05$, which suffers from finite size effects, which affect the stability as well as the numerics. Therefore, a larger $V = 1.5$ is used in the following sections, in order to study the (ρ, T) dependence, and $U = 3.5$ is chosen so that the stripe SC states can be stabilized in both UV-model and U-model.

Note that along with the PDW and mdSC solutions which have the three-legged AF stripes and vertical lines of non-magnetic SC sites, other stripe SC states with the same stripe wave vectors but with a different domain structure can be stabilized. Some examples of such states are schematically depicted in Fig. 5.4. It turns out that the Free energy of these states (e.g.

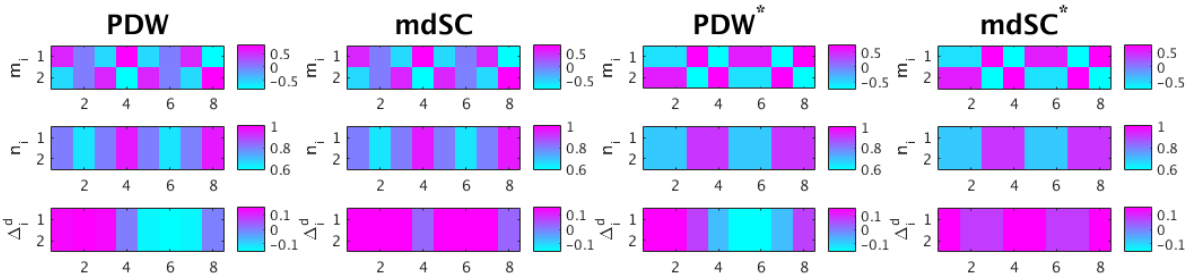

Figure 5.4: Schematic pictures of PDW and mdSC solutions with different domain structures. PDW and mdSC are the ones that have been studied in the previous sections, which come with three-legged AF regions separated by non-magnetic SC lines. PDW* and mdSC* are alternative states which have two-legged AF regions separated by slightly magnetic 2-legged SC regions. Note that PDW has a sign change in Δ_i^d while mdSC does not.

PDW* and *mdSC**) are either degenerate or higher than that of the PDW and mdSC in the parameter regions studied, and therefore not included in the figures in the following sections, for the sake of clarity.

5.2.2.1 ρ *dependence*

The ρ dependence of the stripe SC solution with the UV-model and U-model are studied in Fig. 5.5 and Fig. 5.6 respectively, with the same set of parameters $(U,V,T) = (3.5, 1.5, 0.01)$

The main finding in Fig. 5.5 is that in the UV-model for the given parameter set, the uniform SC is the lowest in energy over the filling region of $\rho < 0.83$, which corresponds to the overdoped region, while both stripe SC states, PDW and mdSC, are the lowest in energy at the filling region of $0.83 < \rho < 0.89$. Once the chemical potential μ exceeds a critical value, the lowest free energy state is the almost half-filled, uniform AF state with almost complete spin polarization (i.e. $m_i \simeq 0.92$), in qualitative agreement with the generic phase diagram for cuprates given in Chapter 1. It is also interesting to note that the PDW order parameter takes its maximum value in each stripe SC solution near the critical filling $\rho^* = 0.82$, below

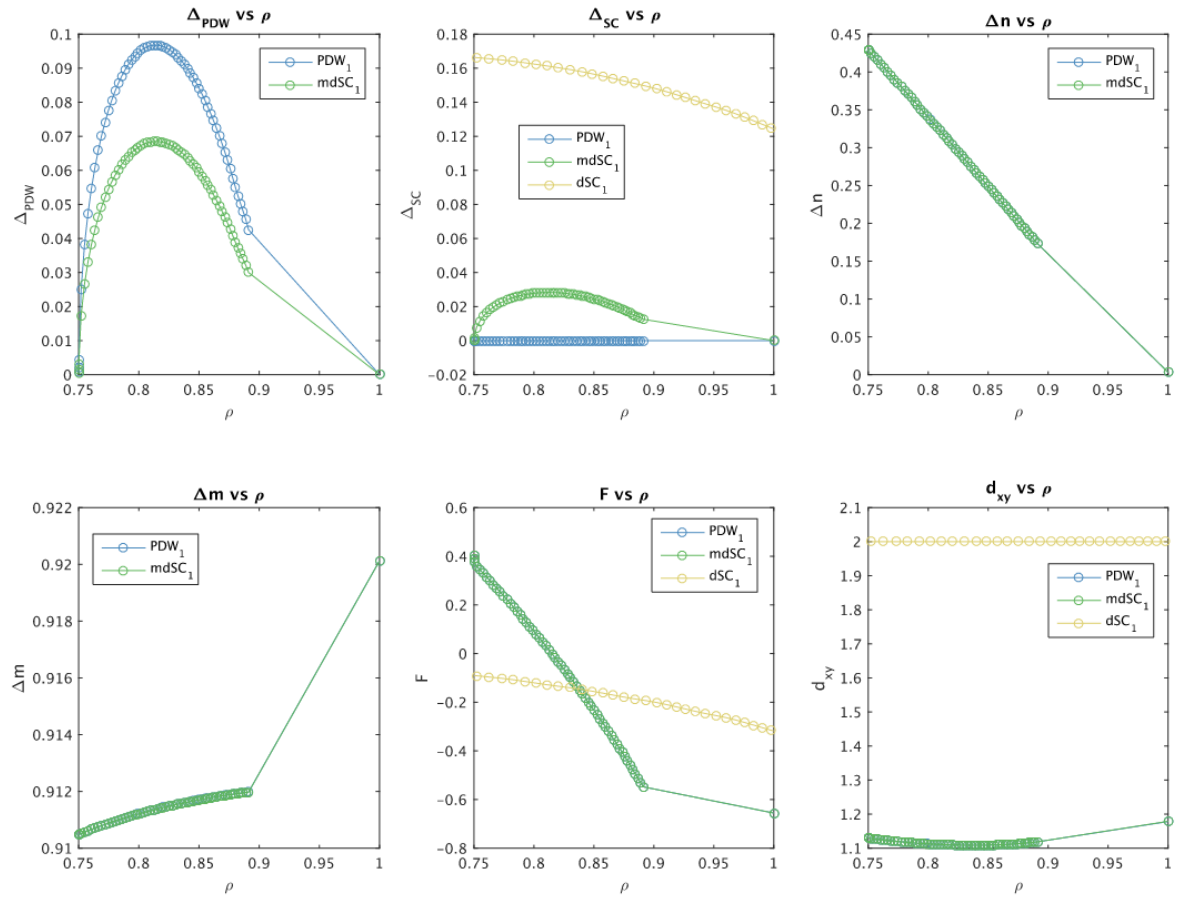

Figure 5.5: The ρ dependence of several parameters describing the PDW, mdSC and uniform d-wave SC (dSC) solutions obtained with the UV-model with $(U,V) = (3.5, 1.5)$ at fixed $T = 0.01$. The subscript 1 represents the UV-model. (Top) The ρ dependence of order parameters Δ_{PDW}, Δ_{SC} and the magnitude of CDW $\triangle n$. (Bottom) ρ dependence of the magnitude of SDW $\triangle m$, Free energy F, and the effective dimension of SC in the system $d_{xy} = 1 + \frac{|\Delta^x_{max}|}{|\Delta^y_{max}|}$ (the further details discussed in the text). Note that a constant increment of the chemical potential, $\delta\mu = 0.02$, is used to trace over the filling region (further details in Appendix A).

which SC becomes the lowest in energy. The effective dimensionality of SC is $d_{xy} \simeq 1.1$ for both stripe SC states obtained with the UV-model, suggesting that quasi 1D-like SC behavior is generic over the studied filling range.

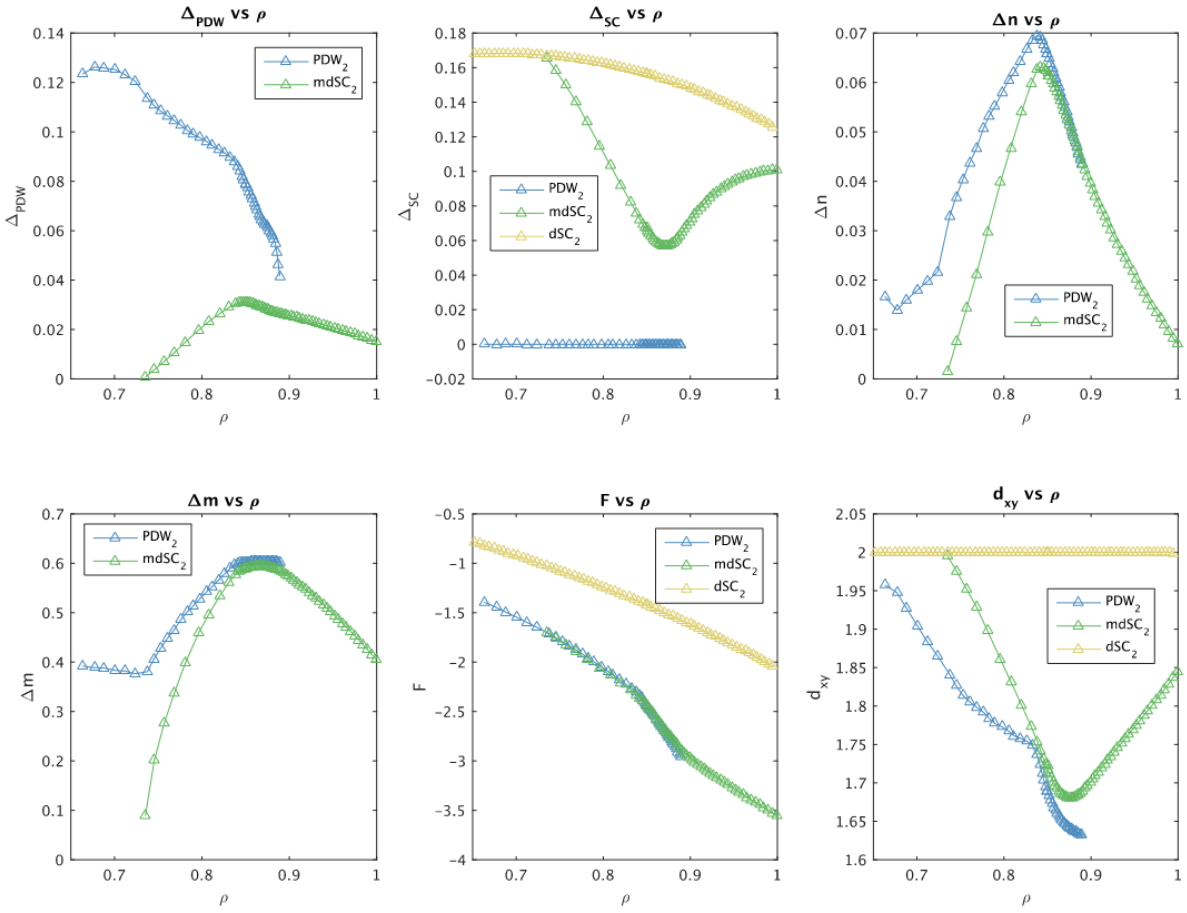

Figure 5.6: analogous to Fig. 5.5, but with the U-model.

The main finding in Fig. 5.6 is that in the U-model for the given parameter set, both stripe solutions are stabilized in a broader region of filling, and their Free energy is lower than that of the uniform dSC state in the entire filling region. Also due to smaller SDW order, the mdSC state at low filling $\rho < 0.75$ has coexsting AF stripes and uniform SC. The effective dimensionality of SC d_{xy} also suggests that at low ρ, SC becomes 2D-like. Note that the parameter set used $(U,V) = (3.5, 1.5)$ is probably not in the physical regime for the U-model, and small $V \leq 1$ is the physical regime for the U-model,, as found in Fig. 5.3, since ignoring

the Hartree shift from the V interaction is only reasonable if V is relatively small. This fact is also mentioned in a previous work[49].

5.2.2.2 T dependence

The T dependence of the stripe SC solution with the UV-model and U-model are studied in Fig. 5.7 and Fig. 5.8 respectively, with the same set of parameters $(U,V,\rho) = (3.5, 1.5, 0.875)$.

The main finding in Fig. 5.7 and Fig. 5.8 is that at $\rho = 0.875$, both stripe SC states have lower free energies than the uniform SC state at low T, in agreement with the finding in the previous section that at $T = 0.01$ stripe SC states are lower in energy than the uniform SC state for the filling range of $0.83 < \rho < 0.89$.

The main difference between the results of the UV-model (Fig. 5.7) and U-model (Fig. 5.7) are that the degeneracy between the PDW and mdSC solutions are lifted at low T in the U-model, where the PDW has lower Free energy than mdSC. In addition, the effective dimensionality d_{xy} suggests that both stripe SC states obtained with the UV-model have quasi 1D-like SC behavior, while both stripe SC states obtained with the U-model have quasi 2D-like SC behavior, and this is generic over the range of T where stripe states are stabilized.

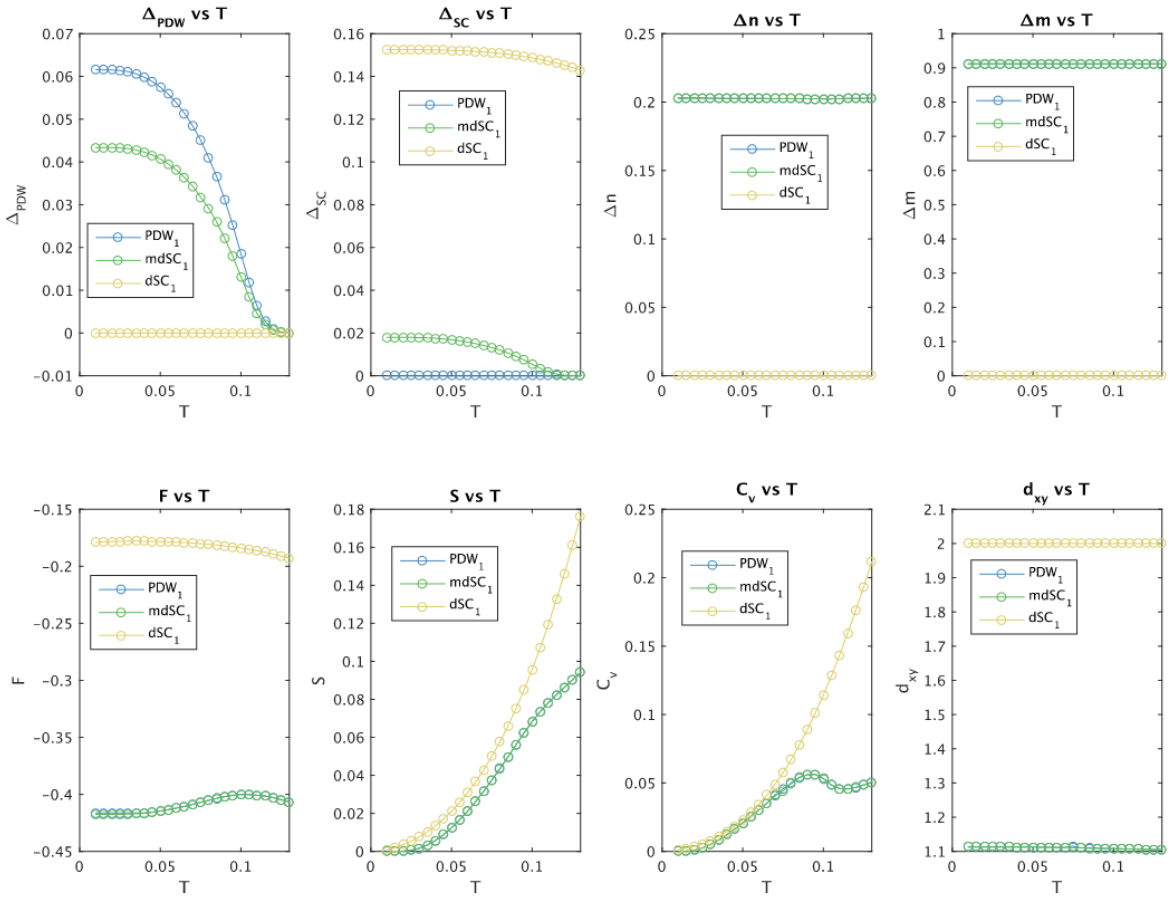

Figure 5.7: the T dependence of the PDW, mdSC and uniform dSC solutions obtained with the UV-model with $(U,V) = (3.5, 1.5)$ at fixed $\rho = 0.875$. The subscript 1 represents the UV-model.

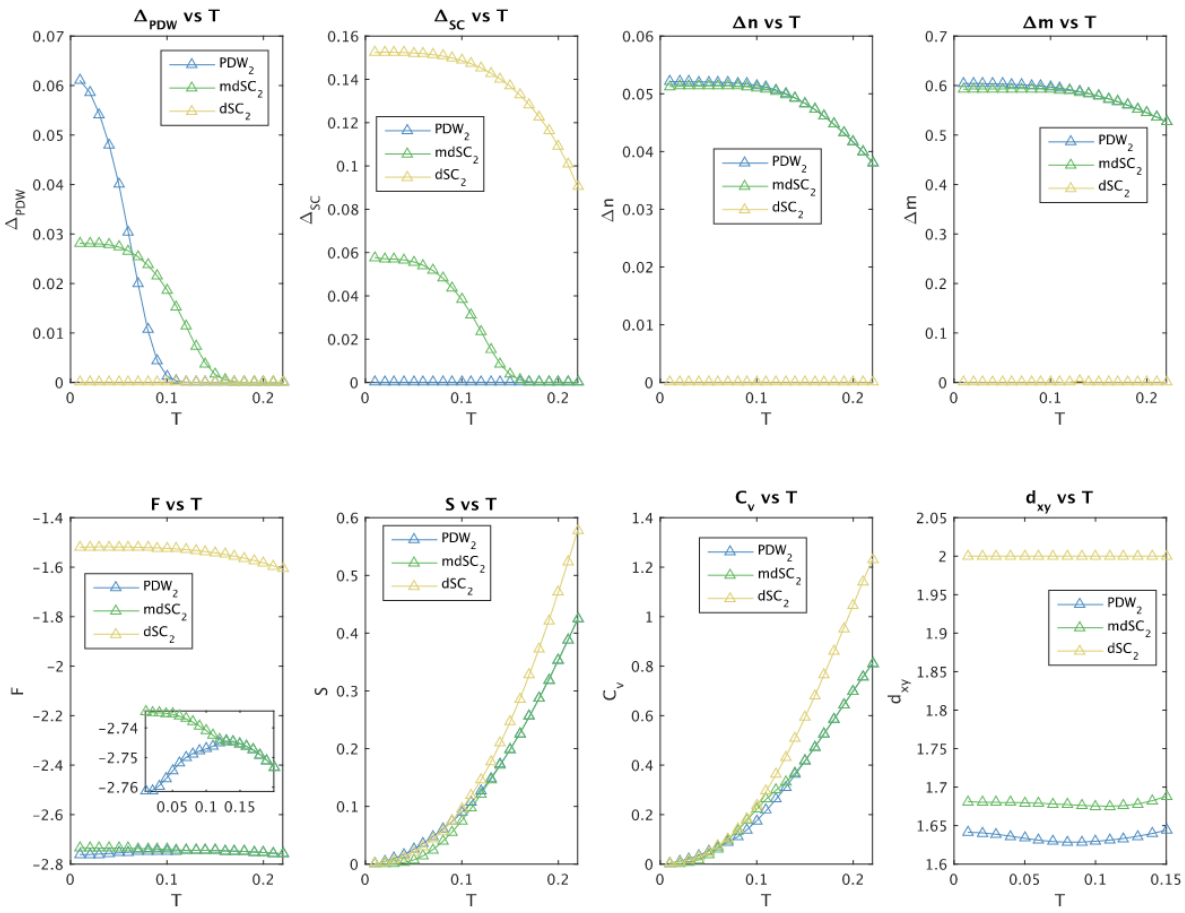

Figure 5.8: similar to Fig. 5.7 but with the U-model. The subscript 2 represents the U-model. The inset in the Free energy plot shows a zoomed-in version which shows the close Free energies for the PDW and mdSC solution.

Chapter 6

Conclusion

The main objective of this thesis is to reproduce and extend previously published works by Loder and others[47, 49, 50], which studied stripe SC states using self-consistent BdG calculation with the UV-model and related models. Specifically, the parts of this thesis which reproduced published works included stabilizing PDW and mdSC solutions with both UV-model and U-model with a set of parameters and characterizing each solution. The parts which extend previous work correspond to mapping out parameter regions where the stripe SC states can be stabilized. Note that the region of doping where PDW order is found to be stabalized is roughly consistent with where striped charge order is found in the generic phase diagram of the cuprates.

In addition, the nature of stripe states with coexisting PDW, CDW and SDW order were studied using non-self-consistent BdG calculation in chapter 4. One conclusion of these results is that the SDW order plays an important role in reconstructing the FS in stripe states, and strong SDW order leads to a completely gapped spectrum in the coexisting PDW state. Therefore, the Fermi arcs (as seen by ARPES in the underdoped cuprates) can be expected only for the states with small SDW.

Interestingly, in chapter 5, self-consistent PDW solutions of the U-model were found to be stable with relatively small SDW order in some regions of parameter space. These PDW states have hole-like FS pockets in the anti-nodal regions, which are roughly consistent with the Fermi arcs seen in the spectral weight function. This is a new promising result in favor for the U-model.

Possible future work includes the self-consistent BdG study with the same models in a magnetic field, where preliminary results (not presented in this thesis) suggest that the stripe SC solutions can be stabilized in a broader parameter region than in zero-field calculation, consistent with previous works[51]. In addition to studying the enhanced stability of stripe SC states in a magnetic field, exploring the possibility of QO is another interesting aspect of finite magnetic field studies. For this purpose, the parameter region found in this thesis, where the PDW solutions of the U-model coexist with small SDW order and hence give rise to small FS pockets, is a promising parameter region to explore.

Appendix A

Convergence method and criteria for the self-consistent BdG calculation

Convergence method

After multiple self-consistent BdG iterations, close to convergence, some oscillatory behavior in the solutions are often observed, preventing the smooth convergence. To achieve smooth convergence, the following relaxation method is implemented.

For a generic self-consistent variable X (e.g. the Hartree shift $\eta_{i,\sigma}$ or SC paring Δ_i^{δ}), the input value for $N+1$ th iteration is defined based on the input and output value in N th iteration,

$$X_{in}^{N+1} = \alpha X_{out}^{N} + (1-\alpha) X_{in}^{N}, \tag{6.1}$$

where $0 < \alpha < 1$ is a weighting parameter, and choosing $0.6 \leq \alpha \leq 0.8$ usually gives smooth convergence.

When running the BdG calculation at fixed filling (e.g. when producing a plot as a function of temperature at fixed filling), the chemical potential needs to be adjusted to achieve the target filling $\tilde{\rho}$. For this the following algorithm is used,

$$\mu^{N+1} = \mu^N + \beta\delta\rho, \tag{6.2}$$

where $\delta\rho = \tilde{\rho} - \rho^N_{out}$ is the difference between the target filling and the output filling, and $\beta > 0$ is a parameter controlling the magnitude of update on μ. Various ways to choose β are possible, such as defining β at each iteration based on $\beta = \frac{\delta\mu}{\delta\rho} = \frac{\mu^N - \mu^{N-1}}{\rho^N_{out} - \rho^{N-1}_{out}}$ or using a regression method to deduce the optimal β based on all the prior filling and chemical potential, but one can set β to be a constant value as long as it is small enough to archive the convergence. Larger β is good when the system is far from the target filling and one wants to adjust the chemical potential in a big step, but near the convergence, one wants to adjust the chemical potential more carefully, although this dependence on the distance from the convergence is already included in $\delta\rho = \tilde{\rho} - \rho^n$ linearly.

Based on these considerations, the following step function definition is used for β;

$$\beta = \begin{cases} \beta_1, \text{ for } |\delta\rho| > \delta\rho^* \\ \beta_2, \text{ for } |\delta\rho| < \delta\rho^* \end{cases}, \tag{6.3}$$

where $\beta_1 >> \beta_2 > 0$ and $\delta\rho^*$ is a threshold value of the distance to the target filling. For example, $(\beta_1, \beta_2, \delta\rho^*) = (0.5, 0.1, 0.001)$ is used for the T-trace plot in Fig **??**.

For the plots given as a function of filling, a more efficient approach is to use values of chemical potential uniformly distributed in a certain range, i.e. $\mu = [\mu_{min} : \delta\mu : \mu_{max}]$, achieve the convergence for each μ, and then calculate the corresponding filling. Some adjustments

in increments of μ are necessary near van Hove singularities or other values where the DOS changes rapidly.

Convergence criteria

The convergence in the self-consistnet BdG calculation X is defined as when all the self-consistent variables are converged to the final values within a certain tolerance δX,

$$|X_{out}^{N} - X_{out}^{N-1}| < \delta X. \tag{6.4}$$

It turns out, however, that checking the convergence in the filling ρ and the Free energy F with a tolerance of 10^{-5} usually guarantees the convergence in all the other self-consistent variables.

Appendix B

Sample pseudo code for the self-consistent BdG calculation

There are some important points to note;

- With the particle-hole symmetry present in the BdG construction, the k-dependent Hamiltonian matrices are constructed and solved for only a half of k-points defined in the reduced FBZ, and for the other half of k-points, the corresponding eigenenergies and wave functions are simply found based on those of the symmetry related k-point, without diagonalization.
- In order to achieve the smooth convergence, a relaxation method is used (the details given in Appendix A).

```
1
2 initial_setting % set the model parameters (t,t',U,V,T) and lattice sizes (lx, ly, Mx,My)
3
4 neighbor_list % generate the indexing of sites & their neighbors, which are used to assin the
      input values to a proper matrix element
5
6 k_list=k_vector_list() % generate the indexing of k-vector and its symmtery related point (
      k_list)
7
8 input_values=intiail_config() % set all the initial configurations (n_in, m_in, Delta_in,
      Hartree_in, mu) which are used to construct the Hamiltonian matrix
```

```
9
10 initialization % initialize all the other variables used with proper dimension
11
12
13 %%% BdG main loop %%%%%%%%%%%%%%%%%%%%%%%%%%%%%%%%%%%%%%%%%%%%%%%%%%%%%%%%%%%%
14
15 count=1;
16 converged=false;
17
18 while(count<=maxcount && converged==false)
19
20     count=count+1;
21
22     % construct k-independent Hamiltonian based on input_values
23     [H_up,H_dn]=H_matrix(input_values)
24
25
26     %=============================================
27     for k_index=1:M/2 % trace over half of all the k-points
28
29
30   %%%% (A1) %%%%%%%%%%%%%%%%%%%%%%%%%%%%%%%%%%%%%%%%%%%%%%%%%%%%%%%%%%%%%%%%%%%%
31         %--define k-point (kx,ky)-----
32         kx=k_list(k_index, 1)
33         ky=K_list(k_index, 2)
34
35
36         %----get k-dependent Hamiltonians by applying k-dependent phase to boundary terms
37         [Hk_up, Hk_dn]=boundary_k_phase([Hk_up, Hk_dn])
38
39
40         %----diagonalize the Hamiltonian to get wavevectors and eigenvalues
41         [Psi_k_up, E_k_up]=eigen(Hk_up)
42         [Psi_k_dn, E_k_up]=eigen(Hk_dn)
43
44         %----------calculate the k-dependent expectation values based on self-consistent
               conditions
45         [n_k, m_k, Delta_k, Hatree_k]=self_const(Psi_k_up, Psi_k_dn, E_k_up, E_k_dn)
```

```
%%%% (A2) %%%%%%%%%%%%%%%%%%%%%%%%%%%%%%%%%%%%
    %——get the symmetry related k−point——
    kx=k_list(k_index,3)
    ky=k_list(k_index,4)

    %——for this k−point, get the wavevectors and eigenvalues without diagonalization by
        using symmetry
    [Psi_k_up2, E_k_up2]=bdg_swap([Psi_k_dn, E_k_dn])
    [Psi_k_dn2, E_k_dn2]=bdg_swap([Psi_k_up, E_k_up])

    %————calculate the k−dependent expectation values based on self−consistent
        conditions
    [n_k, m_k, Delta_k, Hatree_k]=self_const(Psi_k_up, Psi_k_dn, E_k_up, E_k_dn)

%%%%%%%%%%%%%%%%%%%%%%%%%%%%%%%%%%%%%%%%%%%%%%%%%%


end % Done: loop over k−points
%====================================================

%——calculate the expectation values by averaging over contributions from all k−points
[n_out, m_out, Delta_out, Hatree_out]=average_over_k(n_k, m_k, Delta_k, Hatree_k)
rho=mean(n_out) % average charge density (filling)

%——calculate new input_values for the next iteration by relaxation method
[n_in, m_in, Delta_in, Hartree_in]=relaxation(input_values, [n_out, m_out, Delta_out,
    Hatree_out])
mu=adjust_mu(mu, rho, target_rho)
input_values=[n_in, m_in, Delta_in, Hartree_in, mu]


%——calculate Free energy & Order parameters————
F=Free_Energy()
[CDW, SDW, PDW, SC]=order_parameters(input_values)

```

```
    %-----convergence_check (stop the iteration if its converged)-----
    converged=convergence_check(rho, mu, F, CDW, SDW, PDW, SC)


end  % Done: self-consistent loop

%%%%%%%%%%%%%%%%%%%%%%%%%%%%%%%%%%%%
```

Bibliography

[1] E. Fradkin, S. A. Kivelson, and J. M. Tranquada, "Colloquium: Theory of intertwined orders in high temperature superconductors," *Reviews of Modern Physics*, vol. 87, no. 2, p. 457, 2015.

[2] C. Tsuei and J. Kirtley, "Pairing symmetry in cuprate superconductors," *Reviews of Modern Physics*, vol. 72, no. 4, p. 969, 2000.

[3] M. Hashimoto, I. M. Vishik, R.-H. He, T. P. Devereaux, and Z.-X. Shen, "Energy gaps in high-transition-temperature cuprate superconductors," *Nature Physics*, vol. 10, no. 7, pp. 483–495, 2014.

[4] P. Fulde, *Correlated electrons in quantum matter*. World Scientific, 2012.

[5] J. G. Bednorz and K. A. Müller, "Possible high t c superconductivity in the balacuo system," in *Ten Years of Superconductivity: 1980–1990*, pp. 267–271, Springer, 1986.

[6] Y. Kamihara, T. Watanabe, M. Hirano, and H. Hosono, "Iron-based layered superconductor la [o1-x f x] feas (x= 0.05-0.12) with t c= 26 k," *Journal of the American Chemical Society*, vol. 130, no. 11, pp. 3296–3297, 2008.

[7] C. Varma, "Theory of the pseudogap state of the cuprates," *Physical Review B*, vol. 73, no. 15, p. 155113, 2006.

[8] Y. Tokura and N. Nagaosa, "Orbital physics in transition-metal oxides," *science*, vol. 288, no. 5465, pp. 462–468, 2000.

[9] M. Norman and C. Pepin, "The electronic nature of high temperature cuprate superconductors," *Reports on Progress in Physics*, vol. 66, no. 10, p. 1547, 2003.

[10] T. Valla, A. Fedorov, J. Lee, J. Davis, and G. Gu, "The ground state of the pseudogap in cuprate superconductors," *Science*, vol. 314, no. 5807, pp. 1914–1916, 2006.

[11] M. Imada, A. Fujimori, and Y. Tokura, "Metal-insulator transitions," *Reviews of Modern Physics*, vol. 70, no. 4, p. 1039, 1998.

[12] J. Mesot, M. Norman, H. Ding, M. Randeria, J. Campuzano, A. Paramekanti, H. Fretwell, A. Kaminski, T. Takeuchi, T. Yokoya, *et al.*, "Superconducting gap anisotropy and quasiparticle interactions: a doping dependent photoemission study," *Physical review letters*, vol. 83, no. 4, p. 840, 1999.

[13] M. Norman, H. Ding, M. Randeria, J. Campuzano, T. Yokoya, T. Takeuchi, T. Takahashi, T. Mochiku, K. Kadowaki, P. Guptasarma, *et al.*, "Destruction of the fermi surface in underdoped high-tc superconductors," *Nature*, vol. 392, no. 6672, pp. 157–160, 1998.

[14] G. Williams, J. Tallon, E. Haines, R. Michalak, and R. Dupree, "Nmr evidence for a d-wave normal-state pseudogap," *Physical review letters*, vol. 78, no. 4, p. 721, 1997.

[15] T. Timusk and B. Statt, "The pseudogap in high-temperature superconductors: an experimental survey," *Reports on Progress in Physics*, vol. 62, no. 1, p. 61, 1999.

[16] Z. Tesanovic, "The mystery and the mystique," *Nat. Phys*, vol. 7, pp. 283–284, 2011.

[17] A. Damascelli, Z. Hussain, and Z.-X. Shen, "Angle-resolved photoemission studies of the cuprate superconductors," *Reviews of modern physics*, vol. 75, no. 2, p. 473, 2003.

[18] A. Kanigel, M. Norman, M. Randeria, U. Chatterjee, S. Souma, A. Kaminski, H. Fretwell, S. Rosenkranz, M. Shi, T. Sato, *et al.*, "Evolution of the pseudogap from fermi arcs to the nodal liquid," *Nature Physics*, vol. 2, no. 7, pp. 447–451, 2006.

[19] N. W. Ashcroft and N. D. Mermin, "Solid state physics (holt, rinehart and winston, new york, 1976)," *There is no corresponding record for this reference*, pp. 490–495, 2005.

[20] C. Kittel and D. F. Holcomb, "Introduction to solid state physics," *American Journal of Physics*, vol. 35, no. 6, pp. 547–548, 1967.

[21] N. Doiron-Leyraud, C. Proust, D. LeBoeuf, J. Levallois, J.-B. Bonnemaison, R. Liang, D. Bonn, W. Hardy, and L. Taillefer, "Quantum oscillations and the fermi surface in an underdoped high-tc superconductor," *Nature*, vol. 447, no. 7144, pp. 565–568, 2007.

[22] A. Audouard, C. Jaudet, D. Vignolles, R. Liang, D. Bonn, W. Hardy, L. Taillefer, and C. Proust, "Multiple quantum oscillations in the de haas–van alphen spectra of the underdoped high-temperature superconductor yba 2 cu 3 o 6.5," *Physical Review Letters*, vol. 103, no. 15, p. 157003, 2009.

[23] S. C. Riggs, O. Vafek, J. Kemper, J. Betts, A. Migliori, F. Balakirev, W. Hardy, R. Liang, D. Bonn, and G. Boebinger, "Heat capacity through the magnetic-field-induced resistive transition in an underdoped high-temperature superconductor," *Nature Physics*, vol. 7, no. 4, pp. 332–335, 2011.

[24] A. Bangura, J. Fletcher, A. Carrington, J. Levallois, M. Nardone, B. Vignolle, P. Heard, N. Doiron-Leyraud, D. LeBoeuf, L. Taillefer, *et al.*, "Small fermi surface pockets in underdoped high temperature superconductors: Observation of shubnikov–de haas oscillations in yba 2 cu 4 o 8," *Physical Review Letters*, vol. 100, no. 4, p. 047004, 2008.

[25] E. Yelland, J. Singleton, C. Mielke, N. Harrison, F. Balakirev, B. Dabrowski, and J. Cooper, "Quantum oscillations in the underdoped cuprate yba 2 cu 4 o 8," *Physical Review Letters*, vol. 100, no. 4, p. 047003, 2008.

[26] S. E. Sebastian, J. Gillett, N. Harrison, P. Lau, D. J. Singh, C. Mielke, and G. Lonzarich, "Quantum oscillations in the parent magnetic phase of an iron arsenide high temperature superconductor," *Journal of Physics: Condensed Matter*, vol. 20, no. 42, p. 422203, 2008.

[27] J. Singleton, C. de La Cruz, R. McDonald, S. Li, M. Altarawneh, P. Goddard, I. Franke, D. Rickel, C. Mielke, X. Yao, *et al.*, "Magnetic quantum oscillations in yba 2 cu 3 o 6.61 and yba 2 cu 3 o 6.69 in fields of up to 85 t: patching the hole in the roof of the superconducting dome," *Physical review letters*, vol. 104, no. 8, p. 086403, 2010.

[28] B. Ramshaw, S. Sebastian, R. McDonald, J. Day, B. Tan, Z. Zhu, J. Betts, R. Liang, D. Bonn, W. Hardy, *et al.*, "Quasiparticle mass enhancement approaching optimal doping in a high-tc superconductor," *Science*, vol. 348, no. 6232, pp. 317–320, 2015.

[29] S. Badoux, W. Tabis, F. Laliberté, G. Grissonnanche, B. Vignolle, D. Vignolles, J. Béard, D. Bonn, W. Hardy, R. Liang, *et al.*, "Change of carrier density at the pseudogap critical point of a cuprate superconductor," *Nature*, vol. 531, no. 7593, pp. 210–214, 2016.

[30] E. Berg, E. Fradkin, S. A. Kivelson, and J. M. Tranquada, "Striped superconductors: how spin, charge and superconducting orders intertwine in the cuprates," *New Journal of Physics*, vol. 11, no. 11, p. 115004, 2009.

[31] S. E. Sebastian and C. Proust, "Quantum oscillations in hole-doped cuprates," *arXiv preprint arXiv:1507.01315*, 2015.

[32] B. Tan, N. Harrison, Z. Zhu, F. Balakirev, B. Ramshaw, A. Srivastava, S. Sabok, B. Dabrowski, G. Lonzarich, and S. E. Sebastian, "Fragile charge order in the nonsuperconducting ground state of the underdoped high-temperature superconductors," *Proceedings of the National Academy of Sciences*, vol. 112, no. 31, pp. 9568–9572, 2015.

[33] M. Ichioka and K. Machida, "Electronic structure of stripes in two-dimensional hubbard model," *Journal of the Physical Society of Japan*, vol. 68, no. 12, pp. 4020–4031, 1999.

[34] J. Zaanen and O. Gunnarsson, "Charged magnetic domain lines and the magnetism of high-t c oxides," *Physical Review B*, vol. 40, no. 10, p. 7391, 1989.

[35] V. Emery, S. Kivelson, and J. Tranquada, "Stripe phases in high-temperature superconductors," *Proceedings of the National Academy of Sciences*, vol. 96, no. 16, pp. 8814–8817, 1999.

[36] M. Granath, V. Oganesyan, S. A. Kivelson, E. Fradkin, and V. J. Emery, "Nodal quasiparticles in stripe ordered superconductors," *Physical review letters*, vol. 87, no. 16, p. 167011, 2001.

[37] M. Granath, "Band structure of charge-ordered doped antiferromagnets," *Physical Review B*, vol. 69, no. 21, p. 214433, 2004.

[38] M. Granath and B. M. Andersen, "Modeling a striped pseudogap state," *Physical Review B*, vol. 81, no. 2, p. 024501, 2010.

[39] P. Prelovsek and X. Zotos, "Hole pairing and clustering in the two-dimensional t-j model," *Physical Review B*, vol. 47, no. 10, p. 5984, 1993.

[40] S. R. White and D. Scalapino, "Density matrix renormalization group study of the striped phase in the 2d t- j model," *Physical review letters*, vol. 80, no. 6, p. 1272, 1998.

[41] S. R. White and D. Scalapino, "Energetics of domain walls in the 2d t- j model," *Physical review letters*, vol. 81, no. 15, p. 3227, 1998.

[42] S. R. White and D. Scalapino, "Competition between stripes and pairing in a t- t- j model," *Physical Review B*, vol. 60, no. 2, p. R753, 1999.

[43] A. Himeda, T. Kato, and M. Ogata, "Stripe states with spatially oscillating d-wave superconductivity in the two-dimensional t- t- j model," *Physical review letters*, vol. 88, no. 11, p. 117001, 2002.

[44] E. Berg, E. Fradkin, E.-A. Kim, S. A. Kivelson, V. Oganesyan, J. M. Tranquada, and S. Zhang, "Dynamical layer decoupling in a stripe-ordered high-t c superconductor," *Physical review letters*, vol. 99, no. 12, p. 127003, 2007.

[45] M. Raczkowski, M. Capello, D. Poilblanc, R. Frésard, and A. M. Oleś, "Unidirectional d-wave superconducting domains in the two-dimensional t- j model," *Physical Review B*, vol. 76, no. 14, p. 140505, 2007.

[46] K.-Y. Yang, W. Q. Chen, T. Rice, M. Sigrist, and F.-C. Zhang, "Nature of stripes in the generalized t–j model applied to the cuprate superconductors," *New Journal of Physics*, vol. 11, no. 5, p. 055053, 2009.

[47] F. Loder, A. P. Kampf, and T. Kopp, "Superconducting state with a finite-momentum pairing mechanism in zero external magnetic field," *Physical Review B*, vol. 81, no. 2, p. 020511, 2010.

[48] M. Zelli, C. Kallin, and A. J. Berlinsky, "Mixed state of a π-striped superconductor," *Physical Review B*, vol. 84, no. 17, p. 174525, 2011.

[49] F. Loder, S. Graser, M. Schmid, A. P. Kampf, and T. Kopp, "Modeling of superconducting stripe phases in high-tc cuprates," *New Journal of Physics*, vol. 13, no. 11, p. 113037, 2011.

[50] F. Loder, S. Graser, A. P. Kampf, and T. Kopp, "Mean-field pairing theory for the charge-stripe phase of high-temperature cuprate superconductors," *Physical review letters*, vol. 107, no. 18, p. 187001, 2011.

[51] M. Schmid, F. Loder, A. P. Kampf, and T. Kopp, "Disorder induced stripes in d-wave superconductors," *New Journal of Physics*, vol. 15, no. 7, p. 073049, 2013.

[52] M. Zelli, C. Kallin, and A. J. Berlinsky, "Quantum oscillations in a π-striped superconductor," *Physical Review B*, vol. 86, no. 10, p. 104507, 2012.

[53] P. W. Anderson, P. Lee, M. Randeria, T. Rice, N. Trivedi, and F. Zhang, "The physics behind high-temperature superconducting cuprates: the? plain vanilla? version of rvb," *Journal of Physics: Condensed Matter*, vol. 16, no. 24, p. R755, 2004.

[54] J. Hubbard, "Electron correlations in narrow energy bands," in *Proceedings of the royal society of london a: mathematical, physical and engineering sciences*, vol. 276, pp. 238–257, The Royal Society, 1963.

[55] M. Y. Kagan and T. Rice, "Superconductivity in the two-dimensional tj model at low electron density," *Journal of Physics: Condensed Matter*, vol. 6, no. 20, p. 3771, 1994.

[56] J. D. Bazak, "Explorations of a pi-striped, d-wave superconductor," 2013.

[57] T. Nakanishi, K. Yamaji, and T. Yanagisawa, "Variational monte carlo indications of d-wave superconductivity in the two-dimensional hubbard model," *Journal of the Physical Society of Japan*, vol. 66, no. 2, pp. 294–297, 1997.

[58] P.-G. De Gennes, *Superconductivity of metals and alloys (advanced book classics)*. Perseus Books Group, 1999.

[59] S. Baruch and D. Orgad, "Spectral signatures of modulated d-wave superconducting phases," *Physical Review B*, vol. 77, no. 17, p. 174502, 2008.

[60] P. A. Lee, "Amperean pairing and the pseudogap phase of cuprate superconductors," *Physical Review X*, vol. 4, no. 3, p. 031017, 2014.